AFRL-VS-TR-2001-1620

Small On-Board Environmental Diagnostic Sensors Package (SOBEDS)

Robert H. Redus
Marilyn R. Oberhardt
Phil G. D'Entremont
Alan C. Huber

Bronek Dichter
Wallie Everest
David J. Sperry
John A. Pantazis

John O. McGarity
Josef Dalcomo
Scott J. Moran

AMPTEK, Inc.
6 DeAngelo Drive
Bedford, MA 01730

5 January 2001

Final Report

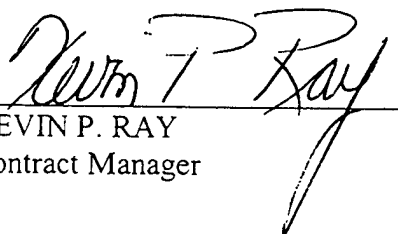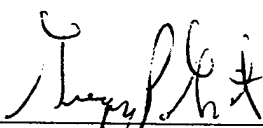20020507 112

AIR FORCE RESEARCH LABORATORY
Space Vehicles Directorate
29 Randolph Rd
AIR FORCE MATERIEL COMMAND
Hanscom AFB, MA 01731-3010

" This technical report has been reviewed and is approved for publication."

KEVIN P. RAY
Contract Manager

GREGORY P. GINET
Chief, SWx Center of Excellence

REPORT DOCUMENTATION PAGE

Public reporting burden for this collection of information is estimated to average 1 hour per response, including the time for reviewing instructions, searching existing data sources, gathering and maintaining the data needed, and completing and reviewing the collection of information. Send comments regarding this burden estimate or any other aspect of this collection of information, including suggestions for reducing this burden, to Washington Headquarters Services, Directorate for Information Operations and Reports, 1215 Jefferson Davis Highway, Suite 1204, Arlington, VA 22202-4302, and to the Office of Management and Budget, Paperwork Reduction Project (0704-0188), Washington, DC 20503.

1. AGENCY USE ONLY *(Leave blank)*	2. REPORT DATE 05-01-2001	3. REPORT TYPE AND DATES COVERED Final

4. TITLE AND SUBTITLE

Small On-Board Environmental Diagnostic Sensor Package (SOBEDS)

5. FUNDING NUMBERS

Contract Number: F19628-95-C-0227
Program Element Number: 63401F
Project Number: 2822
Task Number: GC
Work unit Number: AM

6. AUTHOR(S)

Robert Redus, Alan C. Huber, Phil G. D'Entremont, John O. McGarity,
David J. Sperry, Josef Dalcomo, Marilyn R. Oberhardt, John A. Pantazis,
Scott J. Moran, Bronek Dichter, and Wallie Everest

7. PERFORMING ORGANIZATION NAME(S) AND ADDRESS(ES)

Amptek Inc.
6 DeAngelo Drive
Bedford, MA. 01730

8. PERFORMING ORGANIZATION REPORT NUMBER

9. SPONSORING/MONITORING AGENCY NAME(S) AND ADDRESS(ES)

Air Force Research Laboratory
29 Randolph Rd.
Hanscom AFB, MA 01731-3010

10. SPONSORING/MONITORING AGENCY REPORT NUMBER

AFRL-VS-TR-2001-1620

11. SUPPLEMENTARY NOTES

Contract Manager Kevin Ray/VSBS
(781-377-3828)

12a. DISTRIBUTION AVAILABILITY STATEMENT

Approved for public Release; Distribution unlimited.

12b. DISTRIBUTION CODE

13. ABSTRACT *(Maximum 200 words)*

This report contains the summary of the scientific and engineering work performed during the development of the High Energy Proton instrument (HEP) and of the Low Energy Particle and Dosimetry instrument (LEPDOS). This is a final report on the initial five year portion of the contract effort, which has included the research, development, and fabrication of three flight LEPDOS units, including one with an ESA (electrostatic analyzer), and a flight HEP unit. The second five year portion of the contract will cover spacecraft specific engineering efforts, spacecraft integration, and initial flight support. A separate final report will be written when this effort is completed.

14. SUBJECT TERMS

high energy proton, low energy particle, dosimetry, esa, lepdos, hep

15. NUMBER OF PAGES

16. PRICE CODE

17. SECURITY CLASSIFICATION OF REPORT	18. SECURITY CLASSIFICATION OF THIS PAGE	19. SECURITY CLASSIFICATION OF ABSTRACT	20. LIMITATION OF ABSTRACT
U	U	U	UU

Table of Contents

Illustrations

Tables

Abbreviations

ADC	Analog to Digital Converter
AGS	Alternating Gradient Synchrotron (an accelerator at BNL)
BGO	$Bi_4Ge_3O_{12}$ (a scintillator)
BNL	Brookhaven National Laboratory
EM	Engineering Model
ESA	ElectroStatic Analyzer
CPU	Central Processing Unit
DSP	Digital Signal Processing or Defense Support Program
FPGA	Field Programmable Gate Array
FWHM	Full Width at Half Maximum
GSE	Ground Support Equipment
GSO	Gd_2SiO_5 (a scintillator)
HCL	Harvard Cyclotron
HEP	High Energy Proton Telescope
LEPDOS	Low Energy Particles and Dosimetry Instrument
LSO	Lu_2SiO_5 (a scintillator)
LuAP	$LuAlO_3$ (a scintillator)
LUT	Look Up Table
MCA	MultiChannel Analyzer
PD	Photodiode
PMT	PhotoMultiplier Tube
PWO	$PbWO_4$ (a scintillator)
SOBEDS	Small On-Board Environmental Diagnostic Sensors
TOF	Time Of Flight

D1, D2, D3, D4	Solid State Detectors used in HEP
S1, S2, S3	Scintillation Detectors used in HEP

1 INTRODUCTION

This report contains the summary of the scientific and engineering work performed during the development of the High Energy Proton instrument (HEP) and of the Low Energy Particle and Dosimetry instrument (LEPDOS). This is a final report on the initial five year portion of the contract effort, which has included the research, development, and fabrication of three flight LEPDOS units, including one with an ESA (electrostatic analyzer), and a flight HEP unit. The second five year portion of the contract will cover spacecraft specific engineering efforts, spacecraft integration, and initial flight support. A separate final report will be written when this effort is completed.

The LEPDOS and HEP instruments are part of the SOBEDS (Small On-Board Environmental Diagnostic Sensors) suite of instruments being developed by Amptek, Inc. The purpose of the HEP instrument is to measure the energy spectrum of energetic protons, specifically to obtain a differential spectrum for $25 \leq E \leq 440$ MeV and integral counts for E>440 MeV. The purpose of the LEPDOS instrument is to measure: 1) the lower energy protons and electrons that may cause spacecraft anomalies, specifically protons from 0.7 to 80 MeV and electrons from 5 to >250 keV, 2) the dose and dose rate experienced by spacecraft electronics, 3) particles causing single event effects, and 4) to provide real-time warnings to spacecraft and operators of environmental conditions likely to cause anomalies, such as surface charging and deep dielectric charging. The LEPDOS instrument designs are an outgrowth of previous instruments, while HEP is a fundamentally new design. The HEP development was designated by AFRL/VSBS as a higher priority and required a significantly longer portion of the contract effort.

2 HIGH ENERGY PROTON TELESCOPE

2.1 HEP PROGRAM SUMMARY

Microelectronic components used in spacecraft can be adversely affected by the space radiation environment. In order to understand and predict the performance of electronics in space, it is necessary to accurately measure the radiation environment. Few reliable measurements exist of the most energetic proton population, that above 80 MeV. The operational consequences of this population are important, because these protons penetrate deeply into even the most heavily shielded components and because these particles can cause nuclear interactions, leading to single event effects in microelectronics and thus to operational spacecraft anomalies.

The measurement of high energy protons represents a challenge due primarily to their large range in matter (300 MeV protons have a range of 27 cm in silicon) and to the presence in space of a large omnidirectional flux of penetrating protons (over 10^4 per cm^2-sec at 100 MeV). Because of these and other difficulties, measurements to date have been plagued by large experimental uncertainties. The High Energy Proton telescope (HEP) described here addresses these difficulties through the use of (1) a unique combination of thin semiconductor detectors and a thick segmented scintillation detector, made from a new material, to measure the energy of incident protons, (2) a combination of active coincidence requirements and passive shielding to reduce the response to the large omnidirectional flux, and (3) a flexible on-board data processing system to permit an accurate measurement of effects, such as inelastic nuclear scattering, which lead to a complicated response.

HEP measures the differential energy spectrum of protons from 20 to 440 MeV, in 22 logarithmically spaced energy channels, and the integral flux for protons above 440 MeV. It has an angular resolution of 12° full cone and a geometric factor for high energy protons of 1.7×10^{-2} cm^2-ster. HEP also includes 26 data channels for measuring background events. The instruments consists of two boxes, a 10x8x7 cm sensor head and a 10x10x8 cm electronic box. The total weight is 2.25 kg and total power consumption is as low as 2 watts, depending on the interface. A detailed description of the flight HEP instrument is presented in a paper which has been submitted for publication, "Design and Development of a High Energy Proton Telescope for Space Radiation Studies" by R.H. Redus, B.K. Dichter, M.R. Oberhardt, J.O. McGarity, J. Dalcolmo, S. Woolf, A.C. Huber, J.A. Pantazis, and submitted to Nucl. Instrum. Meth.

2.2 INSTRUMENT CONCEPT

2.2.1 Sensor

The basic configuration of the HEP sensor is sketched in Figure 1. The sensor includes four thin semiconductor detectors, denoted D1, D2, D3, and D4 (front to rear), and the segmented scintillators S1 and S2. PIN photodiodes are used to measure the energy deposited in each of the scintillators. The sensor also includes a cylindrical veto scintillator (S3), passive shielding, and a collimator to reduce the flux from outside the nominal aperture, and a degrader to reduce the flux of low energy electrons and protons.
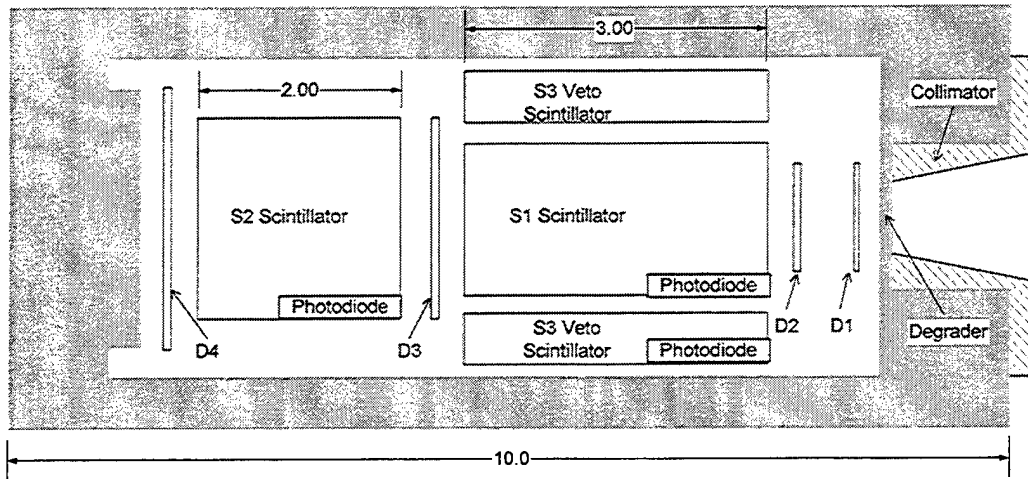
Figure 1. Conceptual drawing of the HEP sensor, in cross-section. All dimensions are in cm.
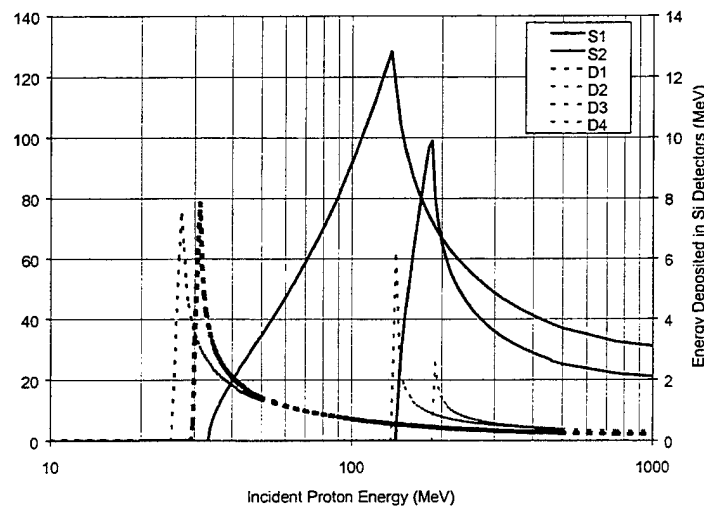
Figure 2. Plot showing the energy deposited in each on-axis detector as a function of incident proton energy. These values were computed using the Janni tables, in the continuous slowing down approximation.

The operation of the instrument can be understood from Figure 2, a plot showing the energy deposited in each on-axis detector as a function of incident proton energy. This plot shows

3

computed mean energy deposition, based on the Bethe-Bloch formula. The semiconductor detectors are used to establish the approximate energy range of the incident protons: a coincident signal from D1, D2, and D3, in anti-coincidence with a signal from D4, implies that the incident proton stopped in S2, the rear scintillator. This implies that the incident proton energy was between 135 and 185 MeV. The amount of energy deposited in the S1 and S2 scintillators establishes the exact energy within this range.

Figure 3 shows the same information but in a different format. The solid line shows the energy deposited in the front scintillator, S1, versus the energy deposited in the rear scintillator, S2, for protons entering from the front. There are three segments to this curve, termed A, B, and C, as noted. Each segment corresponds to a different coincidence pattern from the semiconductor detectors. HEP uses the combination of the pattern of semiconductor detectors that are triggered, along with the amount of energy deposited in the scintillators, to uniquely determine the energy of the incident protons. Protons may also enter from the rear, and these rear-entering protons will both trigger the semiconductor detectors and deposit energy in the scintillators. The dashed line in Figure 3 shows the pattern of energy deposition and detector triggering for these rear entry protons, which can be distinguished from the front entry protons for incident energies below about 300 MeV.
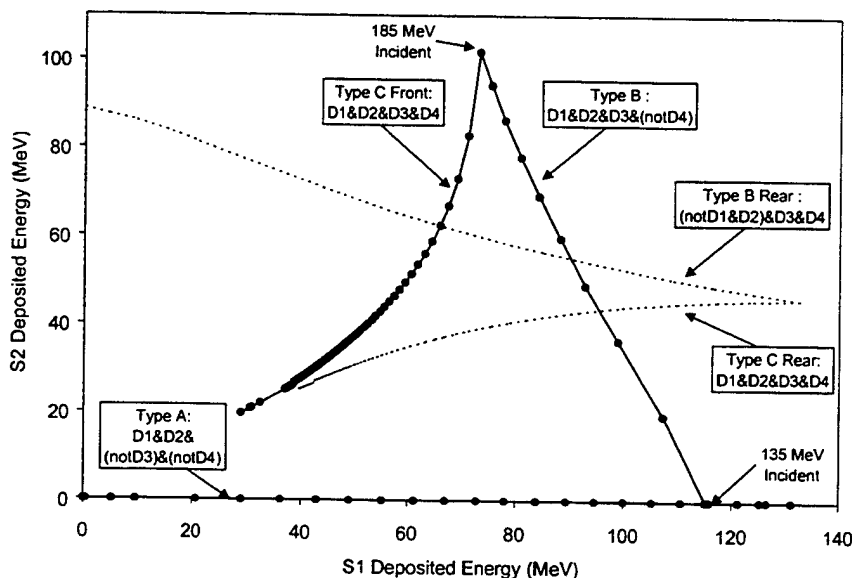
Figure 3. Plot showing energy deposited in S1 versus S2, along with the patterns of triggered semiconductor detectors for each segment. The solid line shows the same data as in Figure 2, but plotted differently. The dots are spaced at 5 MeV incident energy steps, up to 500 MeV. The dashed line shows the pattern of energy deposition for rear entry protons.

The size of the solid state detectors determines the angular acceptance cone, thus permitting the angular distribution of protons to be measured, if the instrument is swept over pitch angles. For type C protons, which must pass through all four detectors, the radii and separation of D1 and D4 define an angular acceptance cone of 12°. The requirement for a simultaneous signal (to within 100 nsec) between the semiconductor detectors ensures that the particles are coming through the desired acceptance cone. The veto scintillator, S3, is used to reject particles which come outside the desired acceptance cone but might otherwise trigger the coincidence logic. A

passive shield is also used, consisting on the sides of 5 mm of Cu, with a proton range of 60 MeV, and in the front and rear of 13 mm of Cu, with a proton range of 100 MeV. This passive shield reduces the omnidirectional flux to minimize accidental coincidences and pulse pile-up. Even with this Cu shield, the maximum flux of protons incident on S3, integrated over the 4π solid angle, is computed from the AP8 model to be 130,000 sec^{-1}. The total flux of particles into S1 and S2 is expected to be over 100,000 sec^{-1}. In contrast, from the omnidirectional AP8 model the average flux of in-aperture protons above 20 MeV is expected to be only 300 sec^{-1}.

Ideally, all in-aperture protons would deposit energy as shown in Figures 2 and 3 and no out-of-aperture protons could trigger the coincidence logic. However, there will inevitably be in-aperture protons that deviate from the pattern shown in Figures 2 and 3, due to (1) statistical fluctuations in the interaction processes and (2) inelastic nuclear scattering events, which are common at these energies. In addition, there is (3) some probability that out-of-aperture protons penetrating the HEP collimator will be accepted by the coincidence logic, and (4) some probability that random, accidental, simultaneous triggering of two or more detectors will generate false signals. These four classes of events form a "background" that must be quantified to obtain an accurate knowledge of the incident spectrum. HEP is designed to minimize these background events but cannot eliminate them. The response of HEP to these event classes has been modeled and measured in ground calibrations. The HEP data processing system is designed to make on-orbit measurements of these "background" event types, allowing correction factors to be determined for these events.

There are three primary means of measuring these background events. First, many of these events produce energy depositions in the S1 and S2 scintillators that do not lie on the curves shown in Figure 3. Up to 20% of the protons passing through HEP will undergo a nuclear interaction, producing an energy deposition pattern deviating from that computed using the Bethe-Bloch formula. For example, if a 160 MeV proton, which would normally stop in S2, undergoes a nuclear interaction in S2, then it will deposit the expected energy in S1 but less in S2. There is a region in the S1S2 plane below segment "B" that corresponds to such nuclear interactions. HEP includes 26 "background" energy channels, each of which can correspond to an arbitrary portion of the S1S2 plane, to measure particles penetrating from the rear, nuclear interactions, and other effects. Second, the same population of off-axis penetrating particles that produce false signals, with both logic pattern and S1S2 deposition matching the in-aperture particles, also produces signals with distinct logic patterns. HEP can therefore return the number of counts that do not match the expected logic, for example returning the counts that have energy deposition consistent with segment "C" above but a logic pattern consistent with "A". HEP will have six patterns, termed "logic masks," which are in simultaneous use, and can be altered by command from the ground. Third, to quantify the fraction of pulses lost due to false vetoes or affected by pulse pile-up, the raw count rates in each detector and for each logic pattern will be measured. The false trigger and false veto rates can be very readily deduced from the measured raw count rates.

5

2.2.2 Electronic Design

Figure 4 is a block diagram of the analog and digital electronics used in HEP. Each detector is connected to analog circuitry to amplify and shape the output pulses. The outputs of the semiconductor detectors and the S3 veto scintillator go to discriminators, which trigger the coincidence logic. If these detectors match a predetermined pattern, within a 100 nsec coincidence window, then the S1 and S2 amplitudes are digitized. The coincidence logic accepts six patterns, termed "logic masks", set by ground command. Crude pulse-height analysis (four levels) is performed on the outputs of the semiconductor detectors to reduce false triggering.
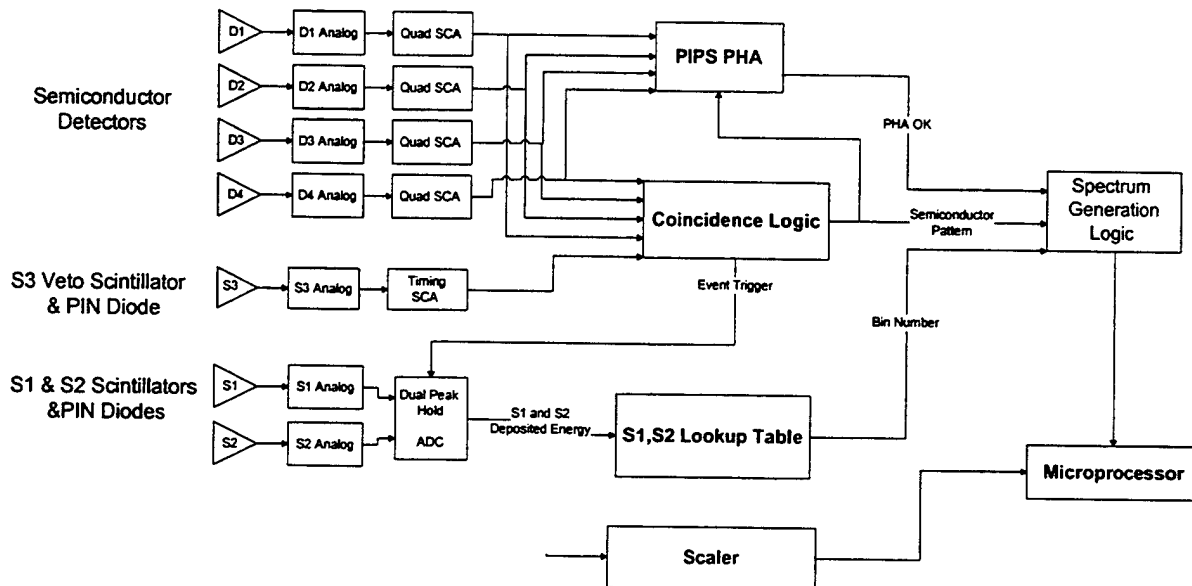
Figure 4. Block diagram of the HEP flight electronics

The S1 and S2 digitizers output the deposited energy with 6 bit resolution. The 12 bit combination is input to the S1S2 Look-Up Table (LUT), which maps the 4096 (S1,S2) values into the 120 data channels. A new LUT can be uploaded from the ground. The combination of channel number, determined from the S1 and S2 values, and coincidence pattern, from the semiconductor detectors, is used by the Spectrum Generation Logic to generate six, 120 channel spectra, if the PIPS PHA indicates the pulse heights were correct.

There are actually two of the 6x120 raw data arrays. At any one time, one is active (recording events) and one is inactive. Every 100 milliseconds, the microprocessor toggles the active array and then reads a subset of these spectra, log compresses the values, and transmits them to the ground. Raw count rates from each of the seven detectors and raw count rates for each of the six logic masks are also measured, read by the microprocessor, log compressed, and transmitted to the ground. These raw count rate numbers can be used for dead time corrections.

The instrument has several operating modes, which determine the subset of the 6x120 element raw spectra that will be transmitted. The details of these modes are still TBD, since the requirements depend on spacecraft specific details, but general concepts and examples can be presented. The 120 data channels can be divided into five, 24 channel blocks. The raw spectrum thus contains 6x5=30 blocks. In Mode 1, HEP might transmit 6 segments in each readout period. The user may command from the ground which 6 of the 30 are to be transmitted. In Mode 2, HEP might transmit 12 segments. This will provide more complete information but at poorer

6

temporal resolution. The minimum data packet size will be 72 bytes of spectral data, corresponding to 3 spectra, along with 15 bytes of counter data, and housekeeping, synch, and checksum information. The minimum packet size is 92 bytes.

In order to obtain pitch angle information with a resolution of 6°, as is desired, it is necessary to read the HEP data within 1/60 of a spacecraft spin cycle. If the spacecraft has a fast spin rate and a low telemetry rate, it will not be possible to transmit all 160 bytes x 60 pitch angle bins = 9600 bytes per spin. In this case, HEP will have to be modified so the microprocessor sums data from each pitch angle bin over multiple spins. Additional operating modes will presumably be required, such as 3 data segments per bin. It is possible for HEP to read out individual cells instead of complete blocks, although this is not supported by the existing software.

2.2.3 Mechanical Design

The overall mechanical design of the HEP sensor consists of a sensor head, approximately 10x8x7 cm, connected via a cable (<36") to an electronics enclosure, a 10x10x8 cm box. The sensor head contains the proton sensor, with the seven radiation detectors, the copper shielding, preamplifier circuitry, and amplifiers. The electronics box contains five boards: an analog electronics board, a digital signal processing board (DSP), a processor board (CPU), an interface board (I/O), and a power supply board. Figure 5 shows the internal layout of HEP.
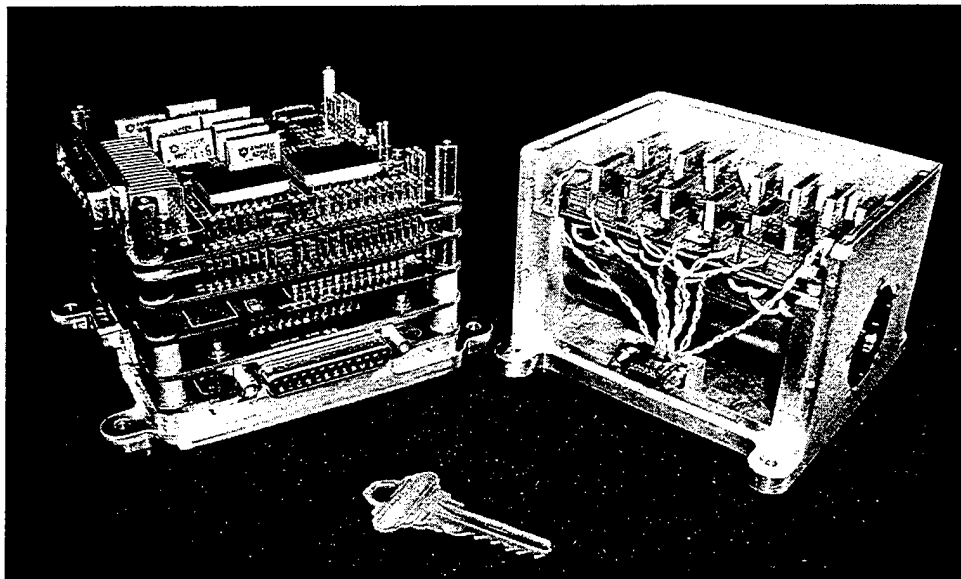
Figure 5. Photograph of the internal layout of the HEP Electronics Box (left) and Sensor Head (right). The copper shield containing the sensors is visible in the Sensor Head, below the preamplifier board. The aperture in the tungsten collimator is visible on the right hand side of the Sensor Head.

2.2.4 Research and Development Program

There were several distinct research and development stages required in the development of HEP during this initial portion of the SOBEDS contract. The design of the sensor assembly is obviously critical to proper operation of the entire instrument, and its design drives the design of the rest of the instrument. Therefore, the first stage concentrated on designing the sensor, particularly on selecting the proper radiation detectors. Selection of the scintillation material was a key concern and required both laboratory experiments and modeling. Selection of the overall sensor geometry and initial calculations of the response to the environment were also carried out. As part of this design and design verification process, an Engineering Model (EM) of the instrument was fabricated to demonstrate the performance, to refine the sensor design, and to determine the specifications for the rest of the instrument. The EM used a sensor head with the detector configuration of the final instrument, but optimized to be readily modified for experimental tests and trade-offs. For electronics, the EM used mostly commercially available NIM and CAMAC components, with some custom electronics and software.

In the second stage, a protoflight sensor head was designed and fabricated to verify and qualify the instrument design. This sensor head used radiation detectors and mechanical components identical to those used in the flight instrument. The analog electronics were prototypes of the flight hardware, while the digital electronics were based on commercial components.

In the third stage (the final one completed thus far), the flight instrument was designed and fabricated. The flight sensor head was virtually identical to the protoflight used in design qualification. The design of the flight electronics was based upon specifications determined during testing of the protoflight unit. The flight electronics include analog pulse shaping circuitry, digital signal processing circuitry (DSP) to select events of interest, a CPU to read the DSP outputs and format them for transmission to the ground, I/O circuitry, and a power supply.

The instrument is completed but has not been tailored to meet the requirements of any particular spacecraft. A future fourth stage will therefore be required to tailor at least the I/O hardware and the software, to conduct the necessary environmental tests, and to carry out the work of spacecraft integration.

2.3 SENSOR DESIGN AND DESIGN VERIFICATION

The initial effort resulted in a baseline design for the HEP sensor. This baseline defined the basic geometry of the sensor, including the size of the detectors and the shielding geometry. The design was based primarily upon the AP8 model of the proton environment, combined with a model of the stopping power of protons to determine instrument response. From the two models, we determined the amount of shielding required to reduce out-of-aperture penetration to an acceptable level, the thickness of detectors required to produce measurable signals, the size of detectors to produce a reasonable geometric factor, and so on. Once the basic geometry of the sensor was defined, the models were used to determine the requirements for the signal processing electronics, including the signal amplitudes, required signal to noise ratios, timing requirements, and so on.

The AP8 model is well known and easily available, but models for the stopping power of protons in the hundreds of MeV range did not address all of the materials planned for use in HEP, nor were they in a convenient form for design work. An initial effort went into the development of software to permit convenient modeling of the proton stopping power. Given this software, the initial design analysis was carried out, the baseline design was developed, and the system requirements deduced from this. An Engineering Model of the sensor was fabricated to verify the models and also to aid in optimizing the selection of the radiation detectors. The S1 and S2 scintillators are key to the proper operation of HEP, so a significant theoretical and experimental effort went into selection of the proper scintillation material.

2.3.1 Stopping Power Model

The stopping power is a key property of any material used in radiation detectors. As a key part of the research reported here, the stopping power of the new scintillator materials was measured and compared with that predicted from existing models. The models were found to accurately describe the stopping power, to within the known limits of the approximations. Based on the experimentally determined corrections, the sensor was designed.

The Bethe-Bloch formula is the basis for analytical expressions for stopping power. It is given by

$$\frac{dE}{dx} = -\frac{4\pi e^4 z^2}{m_e v^2} NZ \left[\ln \frac{2m_e v^2}{I} - \ln \left(1 - \frac{v^2}{c^2} \right) - \frac{v^2}{c^2} \right]$$

where v and ze are the velocity and charge of the incident particle, N and Z are number density and atomic number of the absorber, and I represents the average excitation and ionization potential of the absorber. The calculations reported here used the Janni tables, which are based upon the Bethe-Bloch formula but also include many other important effects. The Janni tables list the stopping power of protons from 100 keV to 500 MeV, with an energy grid fine enough to permit linear interpolation, for a wide variety of elements. However, the Janni tables do not provide results for all elements and are written only for elements.

To accurately describe the experimental data taken here, three steps were required. First, the stopping power and ionization for Gd and Lu, which are not found in the Janni table, were extrapolated from that of Ta, which is in the Janni table. Second, the molecular stopping power for each of the scintillators was computed from the elemental stopping powers found in Janni. Third, since these telescope in practice consist of many layers of material (including air, silicon

detectors, mechanical mounting hardware, etc), software was written to compute energy loss through an arbitrary multilayer target.

To extrapolate from a known element contained in Janni to an unknown, the Bethe-Bloch equation was used. The ionization potential for the unknown elements was computed using formulas in Janni. This extrapolation is valid when the atomic numbers of the two elements are close and was used to compute the stopping power for materials not given by Janni, including Gd and Lu. For these two materials, we extrapolated from Ta, which has similar Z.

To compute the stopping power of compounds from the data given for elements, the Bragg-Kleeman rule was used, in which the stopping power of a compound is a linear sum of the stopping power of its constituent elements (adjusted for the different atom densities of the elements and the compound).

$$\frac{1}{N_C}\left(\frac{dE}{dx}\right)_C = \sum_i \frac{W_i}{N_i}\left(\frac{dE}{dx}\right)_i$$

It should be noted that this is an approximation, and that the actual stopping power of a compound often differs from that of the separate elements, since the molecular energy levels in a compound differ from the atomic energy levels in the separate atoms. This can lead to errors of ±5%. Empirical measurements, such as those reported here, are required to identify such effects. Given the stopping power, proton range is calculated using

$$R(E_0) = R_{0.1} + \int_{0.1\ MeV}^{E_0} \frac{dE}{(dE/dx)}$$

where dE/dx is deduced from the Janni tables, as discussed above, and $R_{0.1}$ is the range of 0.1 MeV protons and is approximately given by

$$P_{0.1}(Z) = 0.06593 + 0.01586\ Z \qquad (mg/cm^2)$$

where Z is the nuclear charge of the element. For a compound, the 0.1 MeV proton range is given by

$$\frac{1}{P_{0.1}(C)} = \sum_i \frac{\omega_i}{P_{0.1}(Z_i)}$$

where ω_i is the weight fraction of the ith element in the compound. This method of calculation ignores proton multiple scattering, which results in a path component perpendicular to the beam direction thus reducing the range. In most cases, for protons with energies above a few MeV, the decrease in range is of the order of 1%.

In the software used to implement the multilayer calculation, two methods are used to compute energy loss. When the range of the particle is less than ten times the thickness of a layer, the energy deposited is computed from the change in the range of the proton. When the range of the particle is at least ten times the thickness of a layer, the energy lost is computed as ΔE = (dE/dx) Δx, where Δx is the thickness of the layer. In principle, both the dE/dx and change in range methods should give the same results, but because of numerical effects, the dE/dx method is more accurate for layer thicknesses much smaller than the range of the particle. This calculation is repeated for each layer of the multilayer target, and for each incident proton energy.

Implementing a convenient user interface for this software was an important part of the software effort, since the design process required repeating calculations with slightly different parameters, to optimize sensor operation. The user interface screen is depicted in Figure 6 and is quite intuitive.

Figure 6. Screen display for software modeling the stopping power of protons.

2.3.2 Initial Design Analysis

Using the software discussed in Section 2.3.1, the baseline sensor design was prepared. The baseline design was very similar to the conceptual design shown in Figure 1. The geometry defined by this analysis is shown in Table 1. A 1 mm copper attenuator, not listed, was selected in front of D1 to reduce the flux of low energy protons and energetic electrons.

Table 1. Geometry of baseline sensor design.

	Material	Shape	Length	Diameter
D1	Si diode		700 μm	0.25 cm^2
D2	Si diode		700 μm	0.25 cm^2
S1	High stopping scintillator	Cylinder	2-3 cm	1.5 cm dia
D3	Si diode		700 μm	1.5 cm^2
S2	High stopping scintillator	Cylinder	2 cm	1.5 cm dia
D4	Si diode		700 μm	3 cm^2
S3	Fast scintillator	Hollow cylinder	2-3 cm	0.6 cm thick
Side Shield	Copper			0.5 cm thick
Front Shield	Copper		1.3 cm thick	
Rear Shield	Copper		1.3 cm thick	

The Si diodes were selected because they are commercially available, rugged devices. These diodes have spaceflight experience in the CEASE instruments and in various instruments flown by Los Alamos National Laboratory. The 700 μm thickness is the greatest thickness routinely available, leading to the largest signal to noise ratio for minimum ionizing particles. The areas of the PIPS detectors were chosen from those commercially available, to provide a good angular resolution (7° half-cone) and a good geometric factor (12x10^{-3} cm^2-ster) for reasonable spacing between the PIPS detectors.

The S1 and S2 scintillator dimensions were chosen to give the correct spacing between the Si diodes. The scintillation material was not yet selected, but for commercially available scintillators with high stopping power, the 2-3 cm thickness was estimated to give a signal of at least 20 MeV for minimum ionizing particles. The S3 scintillator was to be a fast plastic scintillator, chosen to give good timing properties for vetoing out-of-aperture protons. The energy resolution of this scintillator is not important since it acts only as a veto trigger. The thickness (6 mm) was chosen to provide a good signal for most common plastic scintillators.

The shielding design is an engineering trade-off, to (1) reduce the count rate from out-of-aperture protons to an acceptable level, without (2) making the sensor mass excessive for space flight. The 0.5 cm thickness along the sides is equivalent to a proton range of 60 MeV, thus no protons with energy less than 60 MeV can penetrate from out-of-aperture. The 1.3 cm on the front and rear are equivalent to proton ranges of 100 MeV.

With the geometry defined above, it was estimated that the singles count rates in the detectors, and the in-aperture rate of valid protons, would be as shown below, assuming an isotropic AP8 model. The isotropic model is probably reasonable for the singles rates, which are dominated by protons penetrating through the shielding. Isotropies in the proton population are not very important given the shielding geometry. The in-aperture event rate will vary with pitch angle.

Singles Rates (per sec)

D1	D2	D3	D4	S1	S2	S3
1,975	1,975	6,619	22,310	98,310	107,400	138,400

In-Aperture Event Rates (per sec):

A	B	C/D
117.8	9.2	16.8

Based on these count rates, it was determined that the coincidence electronics should have a 100 nsec timing resolution. A fairly extensive analysis of false coincidence and false vetoes was carried out, which showed that the probability of a false positive was extremely small. The probability of a false veto was shown to be about 5%, due largely to the high singles rate in S3.

2.3.3 Engineering Model Design and Fabrication

To test the key hardware components and data handling algorithms intended for use with HEP, and in particular to select the S1 and S2 scintillation material and to verify the stopping power model, an Engineering Model (EM) of the HEP sensor head was manufactured. A cross section diagram of the EM sensor head is shown in Figure 7. The design allowed a flexibility in accommodating the evaluation of a variety of scintillator materials and scintillator light readout devices. The Engineering Model consisted primarily of two, 2 cm dia by 2 cm long cylindrical scintillators. The scintillation signals were read out by PMTs (photomultipliers) (Thorne EMI P25V11 or Hamamatsu R5600) or PIN photodiodes (Hamamatsu S3590 series). The photodetectors were optically coupled to the PMTs via a quartz light guide (Bicron, Inc.), using optical coupling grease. The scintillators and light guides were covered with multiple layers of Teflon tape for maximal light collection. Several different scintillators were fabricated for use in the Engineering Model. Three solid-state detectors (700 μm thick silicon PIPS detectors from Canberra, Inc.) were located among the scintillators to produce trigger signals

12.85°

5.6

46.2

55.7

1.0

136.6

20.0

5.1

S1

34.3

1.2

S2

20.0

1.2

13.0

54.6

All dimensions in mm
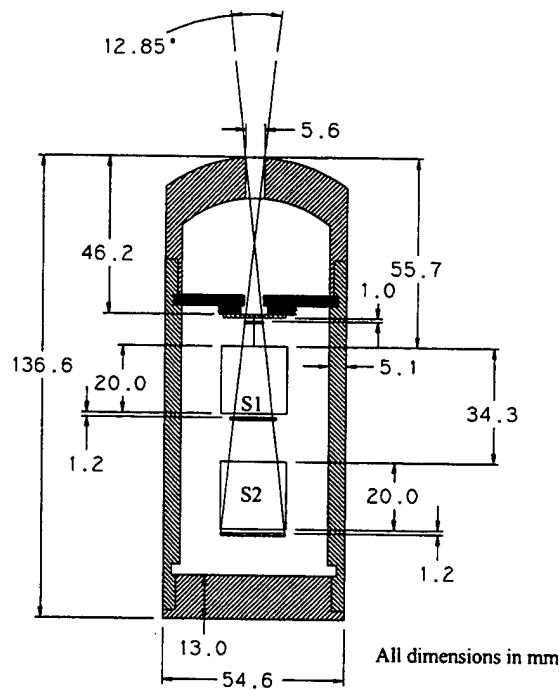
Figure 7. Design of HEP Engineering Model Sensor Head.
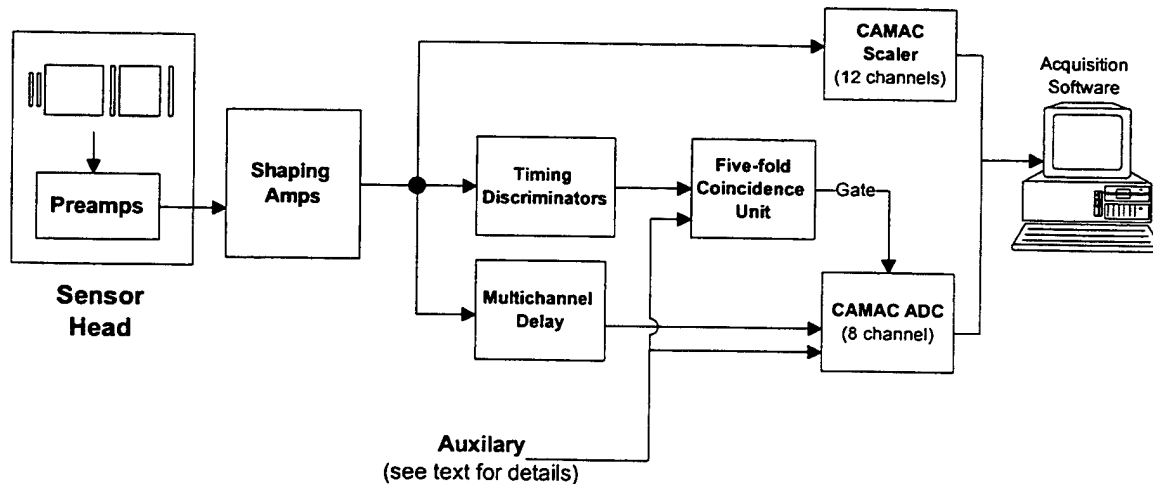
Figure 8. Block diagram of the data acquisition electronics.

The data acquisition system used in these measurements, and in measurements throughout this program, is shown in Figure 8. It consists of three primary components: analog electronics to shape the pulses from the detectors, a multichannel CAMAC ADC to digitize the peak heights for all pulses, and coincidence logic to gate the ADC when a valid event occurred. For each gate generated by the coincidence logic, all six analog inputs, corresponding to the charge generated in each detector, were recorded and stored. In addition to the seven detectors in the particle telescope, described above, auxiliary detectors were used as inputs to the trigger logic. This

14

includes a monitor solid state detector, and at the AGS, a time-of-flight detector discussed in more detail below.

The PMTs were connected, using a 50 Ω terminator, to Ortec 425 shaping amplifiers, without differentiation. The shaped outputs were sent to the ADC while the fast outputs were available for triggering. The photodiodes were connected to preamplifiers, based on the Amptek A250F hybrid, and 0.25 μsec shaping amplifiers made from the Amptek A275F hybrid. This shaping time is much shorter than the noise corner, so adds to the electronic noise, but is necessary to handle the high count rates expected in space from the penetrating omnidirectional flux. The solid state detectors were connected to Amptek A225F hybrids which include both preamplification and pulse shaping. The A225F generates a fast timing pulse, which was sent to the trigger logic, and a shaped pulse, which was sent to the ADC. All of these hybrids are made by Amptek, Inc., and are suitable for space flight: they have low noise, low power consumption, small size, radiation hardness, etc. Custom boards were made to hold these hybrids and to connect them to the sensors.

The fast timing signals were output to the coincidence logic, made from conventional NIM components, including timing single channel analyzers (Ortec 551) and a coincidence module (Ortec 418A). The shaped outputs were sent to a custom, eight-channel, adjustable delay amplifier which insured that all shaped signals arrived at the ADC after the rising edge of the gate signal from the coincidence module. The shaped outputs were digitized by an eight-channel ADC (Ortec AD811). Custom software was used to store these data for subsequent analysis.

The HEP beam experiments were controlled by a computer network. One computer ran the data acquisition program HEPDAQ, which communicated with the CAMAC crate using a SCSI card. HEPDAQ polled the CAMAC crate for valid events accepted by the ADC. If such an event (receipt of a gate from the Coincidence unit by the AD811) occurred, HEPDAQ would 1) transfer the digitized pulse height data for that event to the computer, 2) clear the old data from the ADC and 3) enable the ADC to accept the next event. After every 250 events processed by HEPDAQ, the program would read and clear the data from the scaler.

HEPDAQ stored the data retrieved on an event-by-event basis in a disk file. In order to free up the system resources for CAMAC communications, HEPDAQ performed no data analysis and was strictly a data retrieval and storage program. A second computer ran the data analysis and display program. This program would periodically access the data file written on the data acquisition computer by HEPDAQ, using a local area network, perform simple analysis on the data and update the various displayed spectra and scaler counts.

A third computer ran another program that communicated with the motion control system using the PC-38 card, supplied by the motion system manufacturer. The motion control system included one rotary and two linear stages. The sensor head was mounted on top of the rotary stage, which in turn was attached to a linear stage. This configuration allowed the sensor head to be moved perpendicularly to the beam and rotated with respect to the beam axis. The solid state beam monitor detector was mounted on the second, independent linear stage (the Monitor Stage). This allowed the monitor to be placed in the beam line and directly upstream of the sensor head, whenever desired by the experimenter.

For each experimental run, the stored data file consisted of a list of all eight digitized pulse heights for each ADC gate generated by the coincidence logic. Data analysis software was written to select events, based for example on the pulse heights in the solid state detectors, and to

generate histograms of the pulse heights using only these selected events. These histograms were the basis for the results reported below. In many cases, the parameters of interest were the peak channel and the FWHM. For spectra with a symmetric peak, the centroid channel was computed using Amptek's commercially available MCA software, and the FWHM was computed from the standard deviation about the mean. For asymmetric peaks, the peak channel was identified manually and the direct FWHM computed.
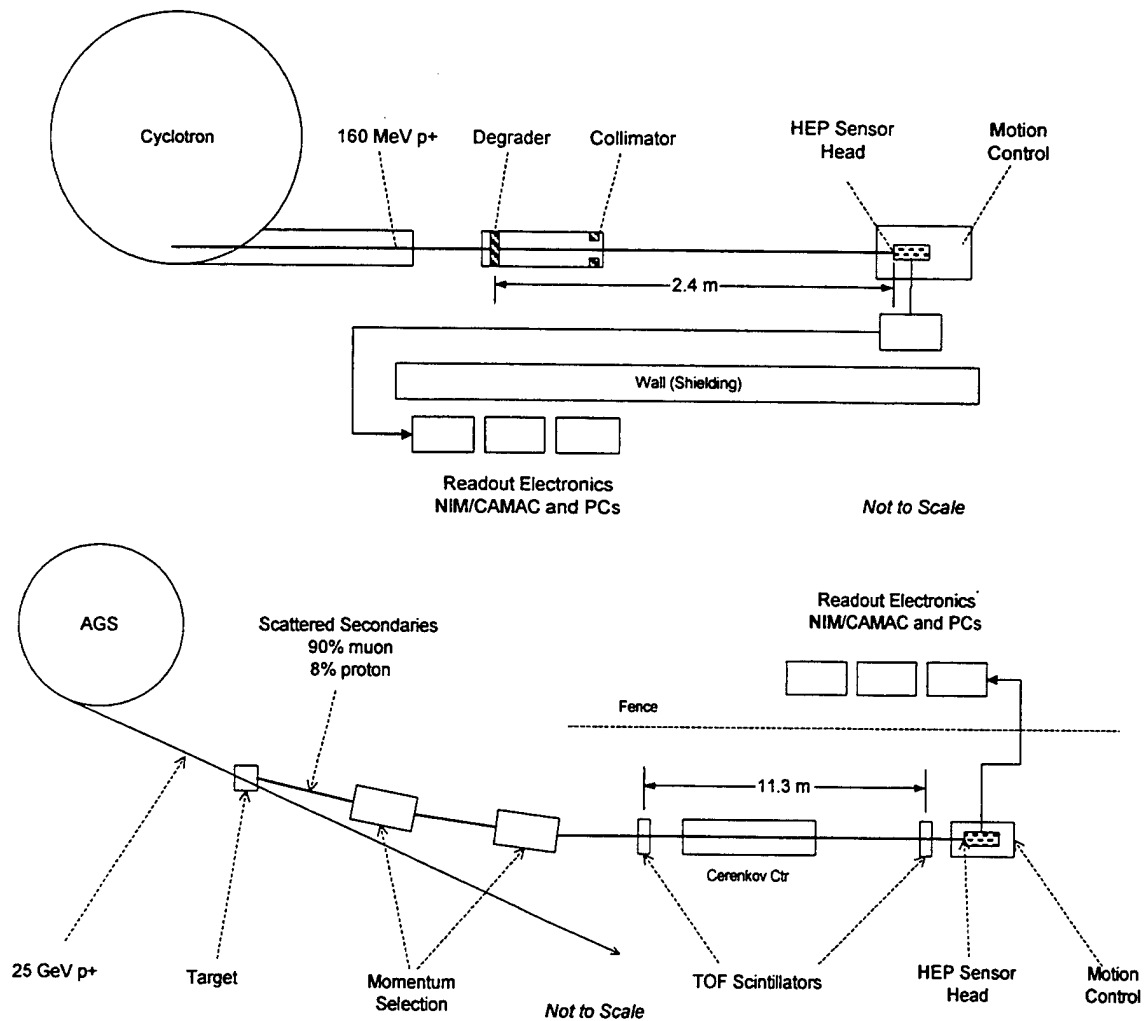

Figure 9. Beam configurations used to calibrate the HEP protoflight sensor head. The Harvard Cyclotron beam, shown on top, was used for energies from 20 to 160 MeV. The B2 Test Beam, from the Brookhaven AGS, was used for energies from 180 to over 2,000 MeV.[1]

2.3.4 Beam Descriptions

Figure 9 shows the configuration of the two beams where most of the data were obtained, both at this preliminary research stage and in later calibrations. The Harvard Cyclotron produces a 160 MeV proton beam. The beam exits the vacuum environment of the accelerator through a thin pressure window and enters the room where the experiment is performed. Just downstream of the window, the beam is directed through a 3.2 cm diameter collimator. Several calibrated degrader plugs (made of lead and Lexan) can be inserted into the collimator tunnel to decrease the incident beam energy. The standard degrader set produces the following mean energies at the exit of the collimator: 29, 37, 45, 54, 73, 92, 111, 131 and 149 MeV. In addition to lowering the mean energy, the degraders also cause additional spreading in energy due to straggling. The lowest energies are associated with the broadest distribution in energy incident on the instrument. The properties of the incident beam, the mean energies and the energy distribution, are well known from previous measurements. The sensor head was located 165 cm downstream of the collimator.

The AGS measurements were conducted at the B2 Test Beam. The AGS primary beam consists of 25 GeV protons, which are incident on a target. The B2 Test Beam consists of the secondary particles produced within this target and includes a variety of particles (muons, protons, positrons, pions, deuterons, tritons, and others) at a wide range of energies. A set of bending magnets and selection windows allows the user to select particles of a particular momentum. The kinetic energies and velocities of the particle species will differ, due to mass differences. To select particles of a given species, a time of flight (TOF) telescope was used to measure the velocity. Proton energies from 184 MeV to 2 GeV were used in the measurements reported here. This corresponds to β from 0.57 to 0.94, and with a TOF distance of 11 m, to transit times of 39 to 64 nsec. For muons at the these momenta, β varies from 0.99 to 0.999 and thus to an essentially fixed transit time of 37 nsec.

The TOF telescope (loaned to us by the PHOENIX group at the AGS) consisted of two plastic scintillator detectors placed 11 m apart and located directly upstream of the sensor. The time difference between the particle passage through the front and back TOF detectors was converted to an analog voltage pulse using a constant fraction discrimination and a time-to-amplitude converter. The TOF signal was used to gate the coincidence logic, to trigger on only the proper species, and as an input to the ADC. This permitted us to directly measure the velocity, and hence energy, of each particle incident on the sensor.

Figure 10 is a plot of the time of flight spectrum, showing the beam composition and indicating the operation of the TOF trigger. The data shown here were taken at a momentum of 2.0 GeV/c, which corresponds to a proton β of 0.90 and a proton kinetic energy of 1.27 GeV. The incident beam is predominantly light particles, which are indistinguishable at this timing resolution (positrons and π mesons have transit times within 90 picoseconds of the muons). K meson have a theoretical transit time of 1 nsec greater than the muons, protons 3.9 nsec, and deuterons 14 nsec. The proton peak has a width of 0.7 nsec FWHM. This includes spreading due to the distribution of incident momenta, admitted by the momentum windows, along with the timing jitter of the system.
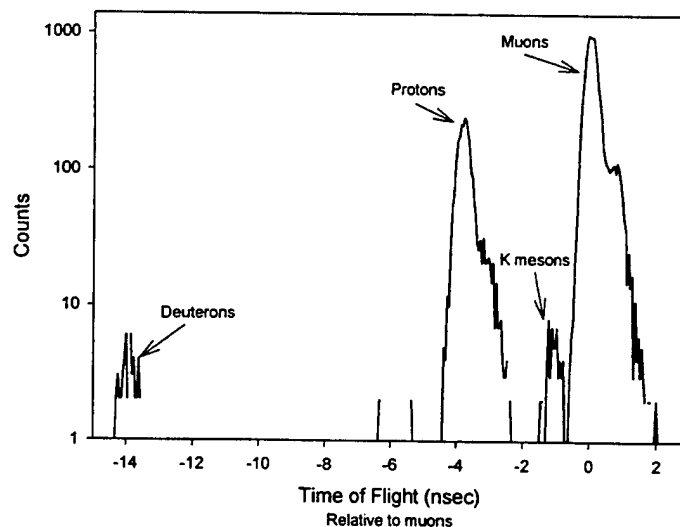
Figure 10. Time of flight spectrum measured at Brookhaven National Laboratory's AGS B2 Test Beam at a momentum of 2.0 GeV/c, showing beam composition and the TOF resolution.

2.4 SCINTILLATOR SELECTION

The choice of scintillator material to be used as the primary HEP detector was critical to the proper performance of the instrument, for this determines the size and signal to noise ratio. The HEP scintillator had to meet three requirements: 1) high density and stopping power, 2) high light output, and 3) short light pulse decay time. The first requirement is necessary because dense scintillator material with a high stopping power can be used to make a small detector. This, in turn, has two benefits: 1) the decreased volume of shielding around the detector will result in a smaller mass of the instrument and 2) the smaller sensitive detector volume will decrease the background counting rate while the instrument is in the inner radiation belt. The second requirement is necessary to achieve good resolution in the measurement of energy deposited in the scintillator by incident protons. The third requirement is important due to the large event rate in the scintillator in the inner radiation belt.

Prior to the SOBEDS contract, scintillator research had resulted in the development of several scintillation materials very promising for the HEP requirements. These materials, which include LuAP, LSO, GSO and PWO, have high density ($\rho > 6$ g cm^{-3}), high atomic number, high light output, and fast decay times. The development of these materials was driven by the needs of medical imaging instrumentation and most of the work on these materials had been done to determine their response to gamma rays, generally below 1 MeV. In the SOBEDS effort, we investigated the properties of interest for charged particle measurements in the energy range of 20 to 2,000 MeV for several of these materials, including LuAP, GSO, PWO and BGO. The properties investigated included proton stopping power, energy resolution, light output, and nuclear scattering effects.

This research demonstrated that the proton stopping power is well described by the Janni model, that the light output for protons and muons is similar to that measured with gammas, that photodiodes can be used for readout, and that an energy resolution of about 15% is obtained for minimum ionizing particles, limited largely by Landau fluctuations in the energy deposition

18

process. The research also clearly demonstrated that GSO was the best available material, that it met the requirements of HEP, and was thus used in the flight sensor.

2.4.1 Stopping Power Measurements

One key experimental goal was to verify the stopping power model discussed above and used as the basis for the instrument design. These stopping power measurements were carried out at the two facilities discussed in Section 2.3.4.

Figure 11 is a plot of the measured and computed proton stopping power using 2-cm scintillators of various materials, over the energy range of 20 to 160 MeV. The LuAP computed values include a 5% correction to the Bragg-Kleeman rule. Note that LuAP has the highest stopping power, requiring the highest incident proton energy before punching through. PWO is next lower, and GSO is the lowest of these three. This is basically a function of the density of the materials, shown in Table 2. The difference in response at the lowest incident energies is due to a change in the low energy absorber used in front of the LuAP scintillator.
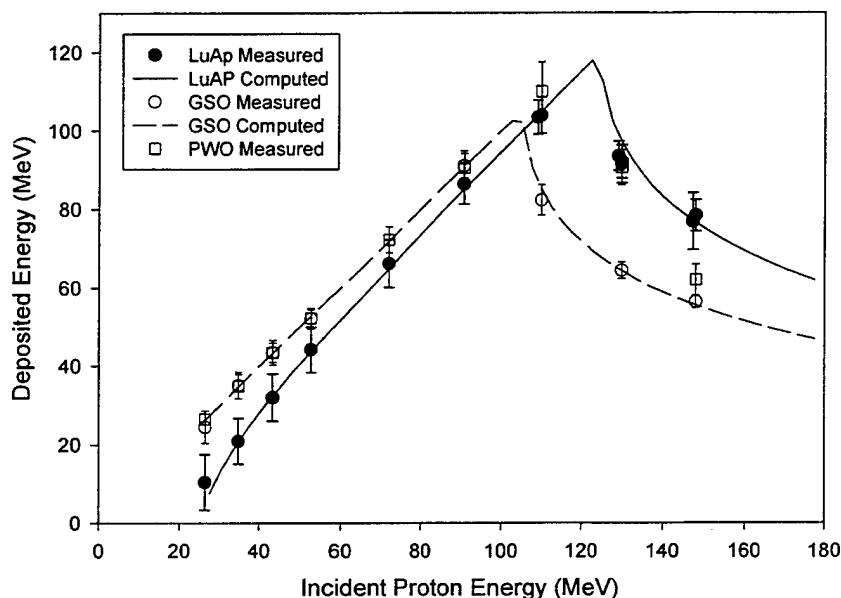
Figure 11. Plot comparing the stopping powers of GSO, LuAP, and PWO scintillators for protons.

A primary conclusion of this effort was that the stopping power model, combining the Janni calculations with the Bragg-Kleeman rule, accurately described these materials to within a few percent, which is the known limit to the approximations. A second conclusion was that the LuAP stopping power was slightly greater than either GSO or PWO.

2.4.2 Light Output

The data acquisition system directly measures the charge generated in the photodetector, rather than deposited energy. To determine the light yield as a function of deposited energy, the MCA was calibrated in units of photoelectrons per channel, by exposing the PIN photodiodes to γ-ray sources (^{137}Cs, ^{60}Co). These produce a well known charge in the silicon detectors, at 3.6 eV per electron-hole pair. A linear regression between these values and MCA channel numbers, for the photopeaks and Compton edges, yielded the number of photoelectrons per channel. Since

the deposited MeV per channel had been determined by the stopping power measurements, the number of photoelectrons generated in the photodiodes per MeV deposited was known. The ^{137}Cs photopeak, at 662 keV, generates 1.8×10^5 photoelectrons in Si. The γ-ray photopeak was in the same MCA channel as 45 MeV deposited energy, implying a signal of over 4,000 photoelectrons per deposited MeV.

Figure 12 is a plot comparing the signal from the photodiode, in units of photoelectrons, versus deposited energy, in MeV. The slope corresponds to 4,470 photoelectrons in the PIN diode per MeV for the front scintillator, S1, and 4,740 photoelectrons per MeV in the rear scintillator. The relationship is highly linear, with a correlation coefficient of 0.997 for S1 and 0.999 for S2, indicating that that the light output is linearly related to the deposited energy for incident proton energies from 20 to 2,000 MeV. Previous research had indicated a slight non-linearity for deposited energies below 30 MeV. The data possibly indicate such a non-linearity, but it is a small effect.
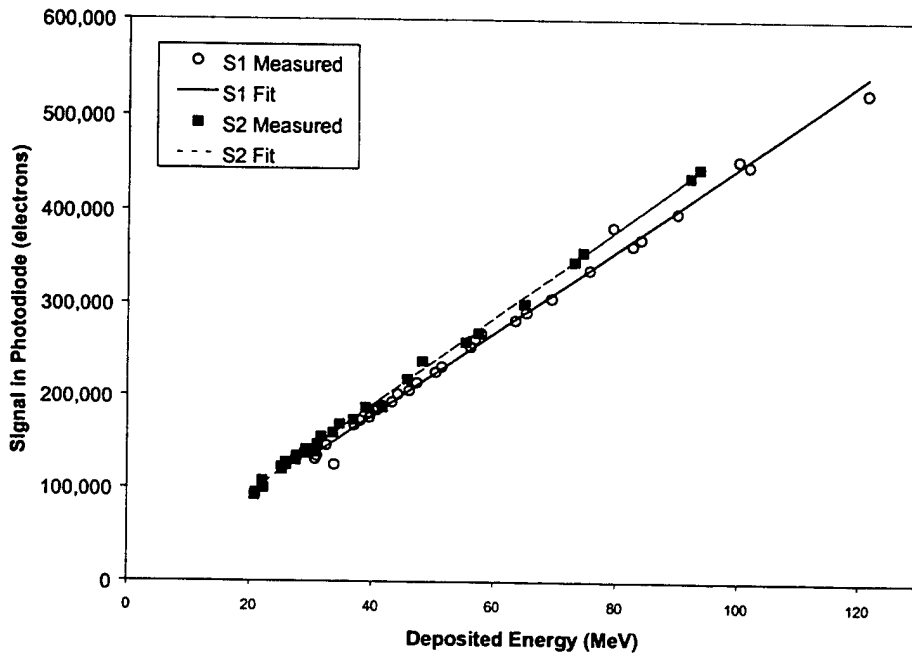
Figure 12. Plot showing the signal generated in the photodiode, in electrons, versus deposited energy, for protons incident on GSO with energies from 20 to 2,000 MeV.

To determine the actual light produced in the scintillator, the absolute light output, requires a knowledge of the efficiency with which photons are collected. This is very difficult to measure directly. It can be estimated, however, since there will be two major loss factors: the quantum efficiency of the photodiode and the geometric light collection efficiency. The quantum efficiency of a silicon photodiode in the wavelength range of interest is typically about 70%. The light collection efficiency for an enclosed volume with walls of reflectivity R and a ratio f of the photodetector sensitive area to the surface area of the enclosed volume is given by

$$\varepsilon_g \cong \frac{f}{[1 - (1-f)R]} \quad .$$

The GSO crystals have areas of about 18 cm^2. The surface area of the photodiode was 0.8 cm^2, giving $f = 0.045$. The crystal was surrounded with a sintered Teflon material having an

20

estimated R of 0.98, resulting in $\varepsilon_g \cong$ 0.70. The efficiency with which photoelectrons will be collected in the photodiode is thus 0.7*0.7=0.49. This would imply that the protons generate approximately 9,000 photons per MeV. Moszynski *et al.* have studied the intrinsic light production by GSO, using γ-rays, and measured a light yield of 6,630±380 photons per MeV. The origin of this significant discrepancy is not known. The LuAP was measured to have higher light output, approximately 9,000 photons per MeV. The PWO was measured to have much lower light output.

2.4.3 Energy Resolution Measurements

Although LuAP had a higher stopping power than GSO, and a higher light output than GSO, its energy resolution was found to be dramatically worse. Spectra from the two scintillators, measured at 90 MeV, are shown in Figure 13. Other laboratory measurements were carried out which demonstrated that there was considerably non-uniformity in the light output of the LuAP crystal. A low energy γ source was moved around the perimeter of the LuAP crystal and the peak height was found to vary dramatically. Because of this effect, and the low light output of PWO, detailed analysis focused on GSO as the best candidate material. Considerable effort went into understanding the energy resolution of the scintillator, since this is a limiting factor in the ability of HEP to measure the energy of protons.
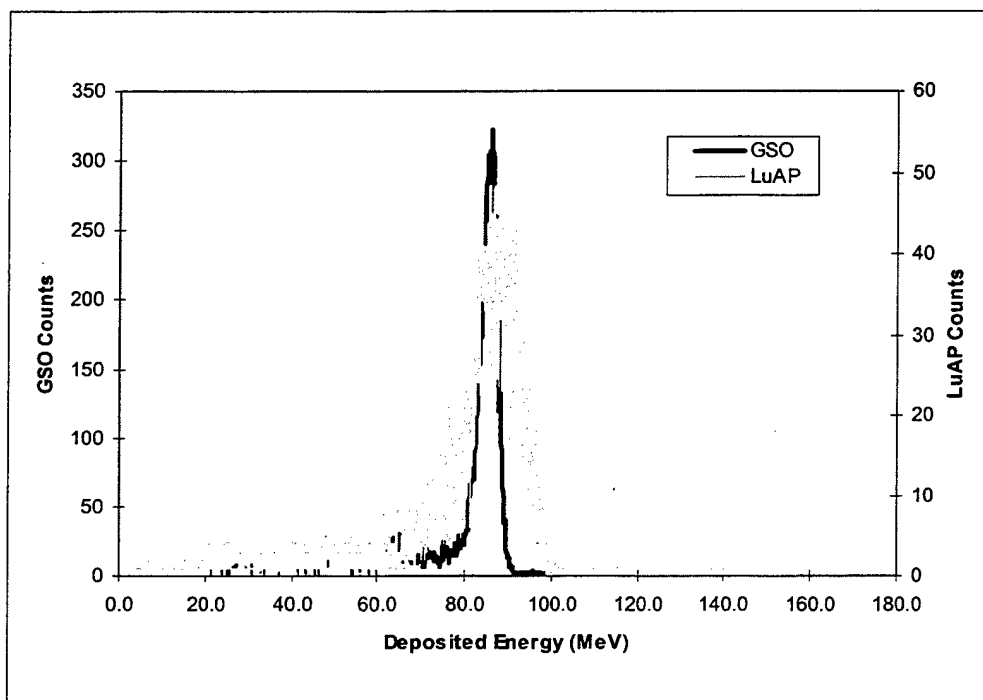
Figure 13. Spectrum of deposited energies measured in GSO and LuAP scintillators, with a PMT readout, using 90 MeV protons at HCL.

To determine the energy resolution of the scintillator it was necessary to consider the significant spreading in the incident energy of the protons. From the width of the TOF peak, at a mean energy of 500 MeV the incident beam energy has a spread of 40 MeV FWHM. However, this only results in a 0.5 MeV FWHM variation in deposited energy, because at these energies dE/dx is a weak function of energy.

There are many possible physical mechanisms responsible for the measured peak broadening. An obvious source is electronic noise generated in the PIN photodiode and the preamplifier input circuitry, noise which is absent with a PMT. Figure 14 shows two spectra taken at 90 MeV incident energy, where the protons stop in the scintillators, with a PIN diode and a PMT. There is no significant difference in the peak width, implying that the electronic noise of the PIN diode does not impact the energy resolution. To measure electronic noise a spectrum was taken with a tail pulser injected into the preamp input, with a width of 0.7 MeV FWHM, as shown. (The small bump in the PIN diode spectrum around channel 210 is due to differences in collimators used with the two setups: protons penetrated a portion of the collimator used with the diode).
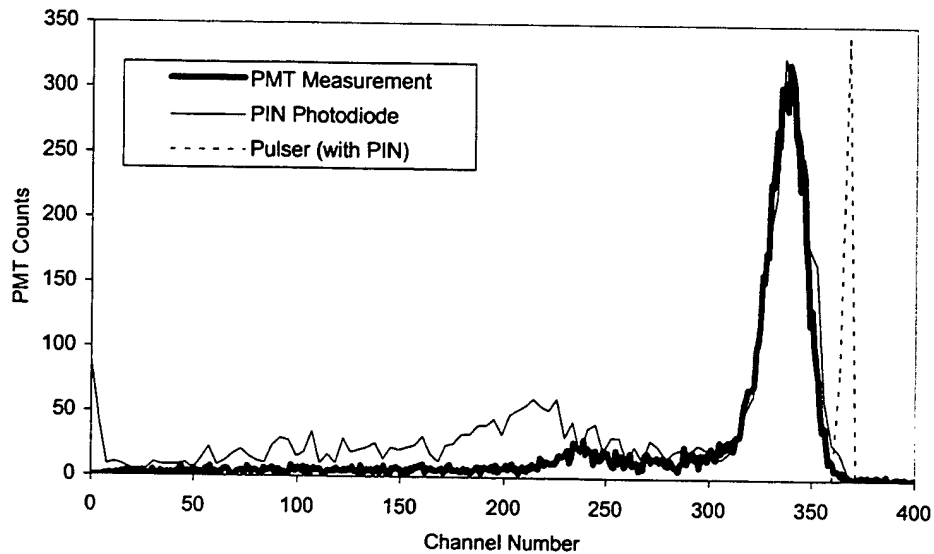
Figure 14. Measured proton spectra taken at 90 MeV with a PMT and a PIN photodiode, showing that the additional electronic noise of the diode adds negligibly to the scintillator resolution. A tail pulse measurement of the electronic noise is also shown.

It is well known that when a charged particle traverses matter, there exist statistical fluctuations in the deposited energy because of variations, from one atomic collision to the next, in the energy transferred to the secondary electrons. The Bethe-Bloch formula gives the mean energy loss per unit volume, but because it is possible to transfer in a single collision much more energy than the mean, there exists a distribution of deposited energies. The exact Landau expression for the distribution of deposited energies is extremely complicated, but a simple analytical approximation was recently developed, in which the probability distribution is approximated as a log-normal distribution. The distribution function, and hence the FWHM, is derived directly from physical parameters, including the Z, A and ρ of the medium and the mass, β, and γ of the incident particle. Figure 15 compares the measured data taken at 500 MeV with the computed probability distribution of the deposited energies. The width and asymmetry of the Landau distribution are known to increase with increasing particle energy. Clearly, this is the major source of peak broadening.
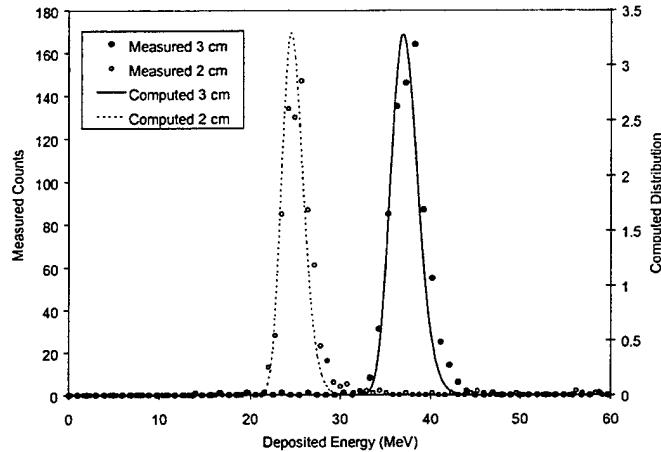
Figure 15. Comparison of measured and computed proton spectra at 500 MeV, showing that the peak width is primarily due to the Landau distribution of secondary electrons.

There are additional sources of peak broadening which doubtless contribute. It is well known that the light yield of a scintillator depends on the energy of the secondary electrons. The same statistical fluctuations in secondary electron production that lead to the Landau distribution will lead to fluctuations in photon production, due to the light nonproportionality. Variations in light collection within the volume of the detector will also contribute to peak broadening. However, these mechanisms are less important for the measurement of penetrating energetic particles than the Landau fluctuations.

2.4.4 Conclusion

A number of scintillator materials were evaluated for use in HEP (see Table 2). Samples for LuAP, GSO, PWO, and BGO were obtained, in approximate "flight instrument" size: 2.0 cm diameter and 2.0 cm long. In the final analysis, GSO was chosen for use on HEP. The primary reasons for the rejection of the other materials were

LuAP: Poor energy resolution (20%) for high energy protons, apparently caused by the manufacturer's inability to produce material of uniform purity,

PWO: Scintillation light output insufficient for use with photodiode and poor energy resolution for high energy protons (20%),

BGO: Long decay time and poor thermal stability, both light output and decay time vary strongly with changes in temperature.

Table 2. Listing of physical properties of studied scintillators.

Property	LuAP (LuAlO$_3$)	GSO (Gd$_2$SiO$_5$)	PWO (PbWO$_4$)	LSO (Lu$_2$SiO$_5$)	BGO (Bi$_4$Ge$_3$O$_{12}$)
Density (g/cm^3)	8.4	6.7	8.3	7.4	7.1
Light Output (phot./MeV)	10,900±1,100	7,900±800	100±11	27,000±2,700	8,060±120
Availability	R&D	Product	R&D	R&D	Product
Rad Hard. (rads)	Not Reported	Protons: 10^7 γ's: 10^9	10^6	Not Reported	10^5-10^6
Resolution (@ 662keV)	9%	11%	Not Reported	13%	11%
Background (cnts/sec-cm^3)	320	None	None	310	None
Hygroscopic	No	No	No	No	No
Light Output: T dependence	Slight	Slight	Not Reported	Not Reported	Strong
Timing: T dependence	None from -10 to +50°C	Not Reported	Not Reported	Not Reported	Strong

2.5 FLIGHT SENSOR UNIT DESIGN, FABRICATION, AND CALIBRATION

2.5.1 Sensor Design and Fabrication

Once the basic design of the sensors was selected and verified experimentally, it was necessary to carry out the detailed design of the flight sensor head. This included a significant mechanical design effort. Optically reflective material must be placed around the scintillators to maximize the optical signal and to eliminate any cross-talk between scintillators. In addition, structures were required which would (1) hold all of the detectors in the correct location, (2) be rugged enough to meet spaceflight requirements, such as shake and vibration, thermal, and out gassing specs, (3) permit the sensor to be assembled and disassembled with relative ease, and (4) keep the total volume small. Some minor changes to the nominal baseline design occurred, due to the requirements of a practical implementation.
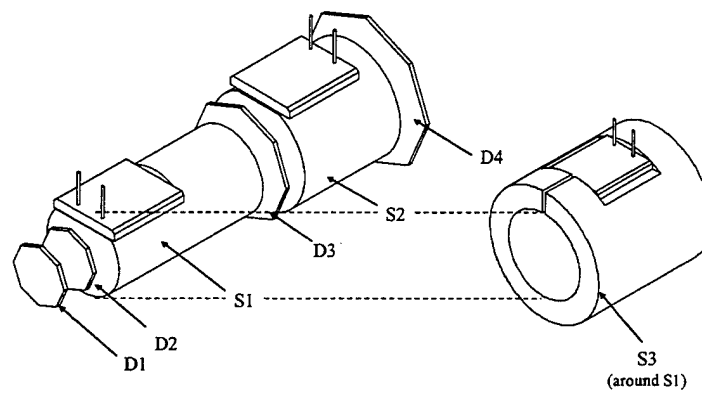
Figure 16. Drawing of the detectors as implemented in the flight sensor head.

Solid State Detectors

Use of the solid state detectors was relatively straightforward. For D3 and D4, 700 µm thick PIPS detectors were obtained from Canberra, Inc. For D1 and D2, custom 500 µm thick ion-implanted detectors were obtained from EG&G Ortec. In the Canberra detectors, the electrically active area extends approximately 1.2 mm beyond the nominal area specified in the data books, which is measured using α particles. For D3 and D4, the additional area is not important. For D1 and D2, instead of the desired 25 mm^2 active area, the electrically active area was 50 mm^2, which dramatically affected the response. Custom detectors were therefore obtained with a true 25 mm^2 electrically active area. Both types of detector are mounted by the manufacturer. Amptek developed a structure which would hold the mounted detectors along the HEP axis, ruggedly, with electrical contacts coming through the shield, which prevents optical photons from reaching the active area of the diodes but which permits protons to pass through the active region with negligible attenuation.

Scintillators

As discussed above, the S1 and S2 scintillators were made from Gd_2SiO_5 (GSO) while the S3 scintillator was made from a fast plastic material, BC-428. We used photodiodes (PD) for optical readout, instead of the more conventional photomultiplier tubes (PMT). PMTs have less noise, but have several significant practical disadvantages. Moreover, as shown in Figure 14 the additional noise of the PD is negligible compared with the scintillator's intrinsic resolution. The PMTs practical disadvantages include 1) its large size, which requires either additional shielding

mass or decreased shielding, 2) the necessity for high voltage, 3) higher power consumption, and 4) sensitivity to magnetic fields. The PD was clearly a superior choice given the practical considerations of space instrumentation and the relatively large optical signals generated in the scintillator by energetic protons.

In order to obtain a good signal to noise ratio, it is critical that the maximum number of photons interact in the PD. This requires good optical coupling of the PD to the scintillator, and a good optical reflector around the scintillator. To obtain good optical coupling, the scintillators were fabricated with a flat surface onto which the PD could be coupled, as shown in Figure 17. The photodiodes, which are commercially available from Hamamatsu, Inc., were epoxied to the scintillators by Bicron, Inc., using space-flight qualified materials and procedures.

For any interaction in the scintillator, with photons emitted isotropically, there is only a small solid angle with photons directly incident on the PD. The scintillator must be surrounded by a reflective material, so that the photons may be reflected (sometimes many times) and still collected. The optical reflector chosen for use in HEP is Spectralon, a sintered Teflon with a reflectance exceeding 99% for optical wavelengths from 300 to 1800 nm. Each of the scintillators was surrounded by at least 1 mm of Spectralon, to obtain the necessary reflectance. Because S1 is surrounded by S3, there was concern of optical cross-talk between the two, so a metallic layer was inserted between the S1 and S3 optical reflectors. In tests at HCL, no optical cross-talk was observed. Figure 5 is a photo of the S1 and S3 scintillator stack, showing the flight scintillator, photodiodes, and Spectralon reflectors. A penny is shown for comparison. The outside diameter of the largest reflector is 3 cm. The tight geometry is clearly visible in this photo.
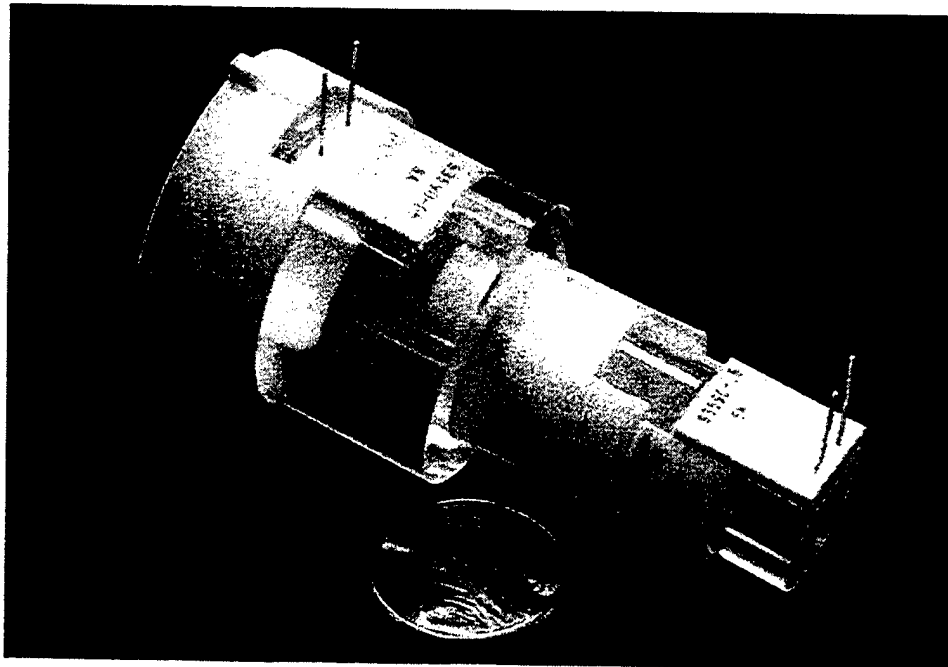
Figure 17. Photograph of the S1 and S3 sensor stack, showing the scintillators, photodiodes, and optical reflectors.

Sensor Assembly

The complete sensor assembly, required to hold the radiation detectors in place, is a complex mechanical arrangement, as shown in Figure 18. An ellipse is drawn around the complete assembly. Figure 18 is an exploded drawing, showing (a) the D1 and D2 assemblies, (b) an assembly containing S1, S3, the PIN diodes, and the Spectralon reflectors, (c) the D3 assembly, (d) the S2 assembly, and (e) the D4 assembly.
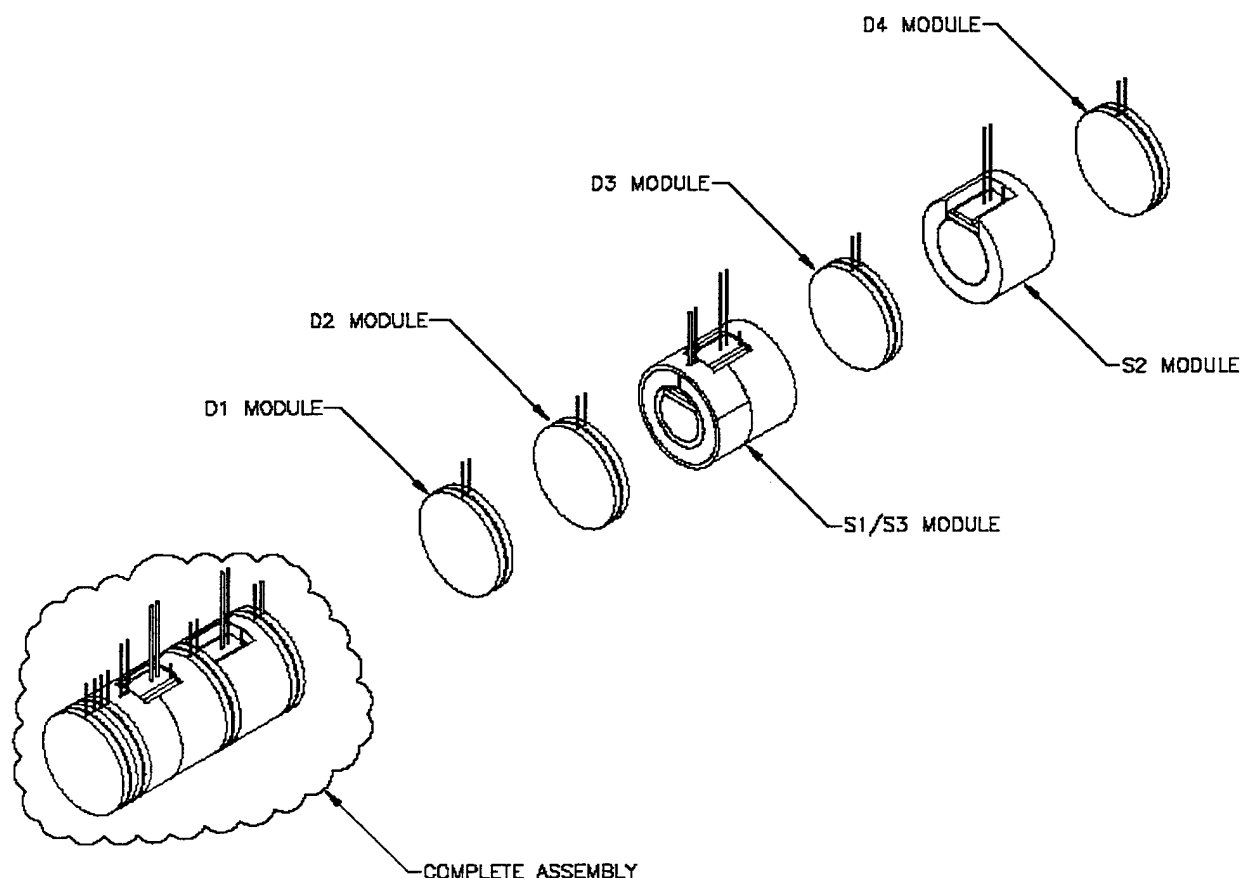
Figure 18. HEP sensor assembly drawing.

2.5.2 Analog Electronics

The analog signal processing electronics used with the sensors is divided between the Sensor Head and the Electronics Box. The Sensor Head contains the preamplifiers and the first amplifier stage. The Electronics Box contains pulse shaping and digitization components.

The four PIPS detectors use identical analog circuitry, shown in Figure 19. The detector output is passed to an Amptek A225F hybrid preamplifier and shaping amplifier. The fast timing output of the A225F is sent to an Amptek A275F hybrid amplifier with additional pulse shaping. The output of the A275F is a fast analog signal, with a measured risetime of 75 nsec, a falltime of 300 nsec, and amplitude of about 1 V/MeV. These hybrids are located on the preamplifier board in the sensor head, so that relatively large signals are sent across the cable to the electronics box. In the electronic box, the A275F outputs go to Amptek 9405 hybrid comparators. The fast discriminator triggers the coincidence logic, while the quad discriminator outputs, which provide rough pulse height analysis, go to the PIPS PHA processing logic.

27
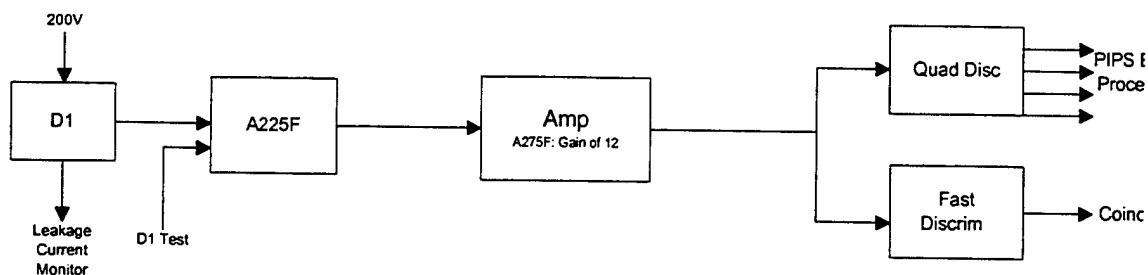
Figure 19. Analog electronics chain used with the four PIPS detectors.

The S1 and S2 scintillator outputs use identical analog circuits, shown in Figure 20. The output of the PIN diodes goes to an A250F hybrid charge sensitive preamplifier. The preamp output goes to a 5 pole pseudo-gaussian shaping amplifier, with a shaping time constant of 0.25 μsec, implemented using A275F hybrids. This shaping time was chosen as a trade-off between the electronic noise, which is reduced at longer shaping times, and pulse pile-up, which is reduced at shorter shaping times. The output of the shaping amplifier is sent to a circuit that captures and digitizes the peak amplitude. This will be used by the DSP circuitry, to determine in which of the 48 channels the count occurred. The digitization is initiated by the coincidence circuitry.
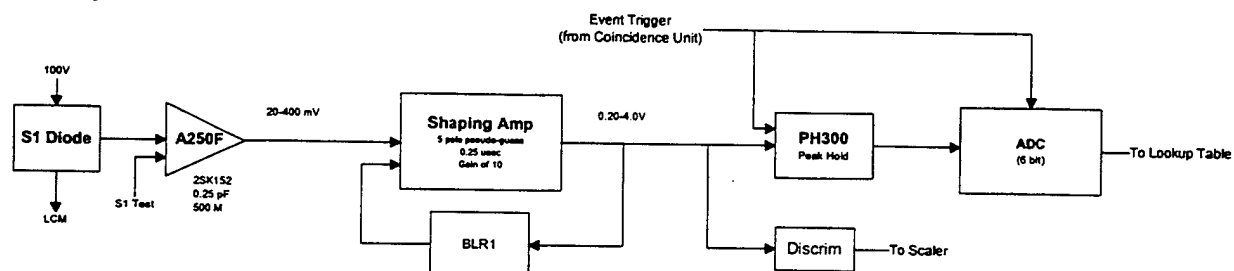
Figure 20. Analog electronics used with the S1 and S2 detectors.

The S3 circuit is similar to the S1 and S2 circuits. It uses an A250F hybrid preamplifier and a pseudo-gaussian shaping amplifier, but with a 0.1 μsec shaping time constant, giving a pulse risetime of 200 nsec. However, the output is connected to a timing discriminator instead of a digitizer. A crossover timing discriminator was used, with a measured timing resolution of <20 nsec FWHM. Using a shorter shaping time increases the noise, which actually degrades the timing resolution, since the resolution of a crossover timing discriminator depends on noise.

2.5.3 Protoflight and Flight Sensor Calibration

During the second stage in the HEP R&D program, the detailed design of the flight sensor head was carried out. Two identical sensor heads were fabricated to this design. The first sensor head completed was designated the "protoflight" sensor head and was used to verify the design and for a very thorough calibration and test program. Once this was completed, the second was completed and was designated the "flight" sensor head and underwent a more limited test program. Both sensor heads are identical, but the protoflight head has undergone significantly more handling. The completed sensor head is shown in the photograph in Figure 5.

The most important measurements were conducted by the Amptek staff and personnel from AFRL/VSBS at the Harvard Cyclotron and at the Brookhaven National Laboratory AGS accelerator. The purpose of the work was to evaluate the performance of the HEP protoflight

sensor head when exposed to in-aperture proton beams with energies between 20 and 2,000 MeV, to calibrate the instrument over this energy range, and to measure the response of the instrument to in-aperture protons experiencing nuclear interactions and to penetrating out-of-aperture protons.

Experimental Apparatus

The experimental apparatus combined the protoflight sensor head (including sensors and preamplifiers) with a breadboard of the analog electronics and external electronic modules for digital signal processing. The use of external electronics permitted the work on the sensor head to proceed independently and in parallel to the work on the development of HEP digital electronics. The overall experimental apparatus used at this stage was similar to that used in the previous research, the scintillator selection measurement. This apparatus was presented in Figure 8 and discussed in the text. The major difference is that, in the early work, all of the analog electronics (including preamps and shaping amps) used external, NIM or custom components. These calibrations used circuitry like that planned for flight. The protoflight sensor head contains, in addition to the sensors, preamplifiers and a portion of the shaping amplifier circuitry. The outputs of the sensor head were sent to a breadboard version of the analog board, containing the rest of the shaping amplifier circuitry. Because the external electronics were located outside of the beam line for personnel access, a distance of up to 100', the analog breadboard included buffer circuits, not intended for the flight boards, to drive the 100' coaxial cables.

In-Aperture Instrument Response

Plots of the measured response of the instrument to the in-aperture incident protons are shown in Figure 21, 22, and 23. Figure 21 compares the energy deposited in the S1 and S2 scintillators with that computed using the Janni model. Figure 22 shows the same data, but it shows the distribution in the S1S2 plane, and also shows the rear entry data. In both figures, the error bars represent the total measured FWHM of the peaks, which includes spreading due the width of the incident beam. The instrument response is much narrower. Figure 23 shows the PIPS data. In all cases, excellent agreement is found between the measurements and the model.
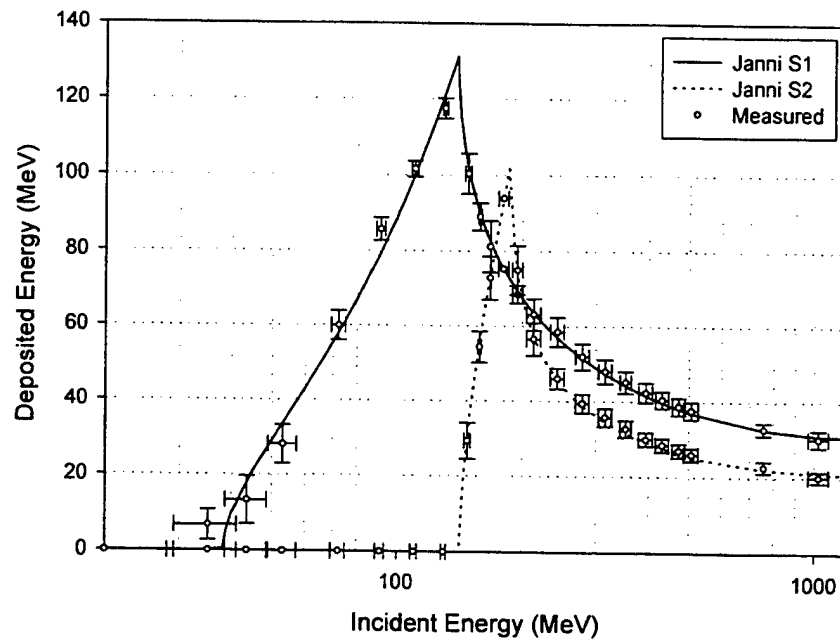
Figure 21. Plot comparing the computed response of the HEP scintillators to that measured at Harvard and Brookhaven, using the protoflight sensor head, identical to the flight sensor head.
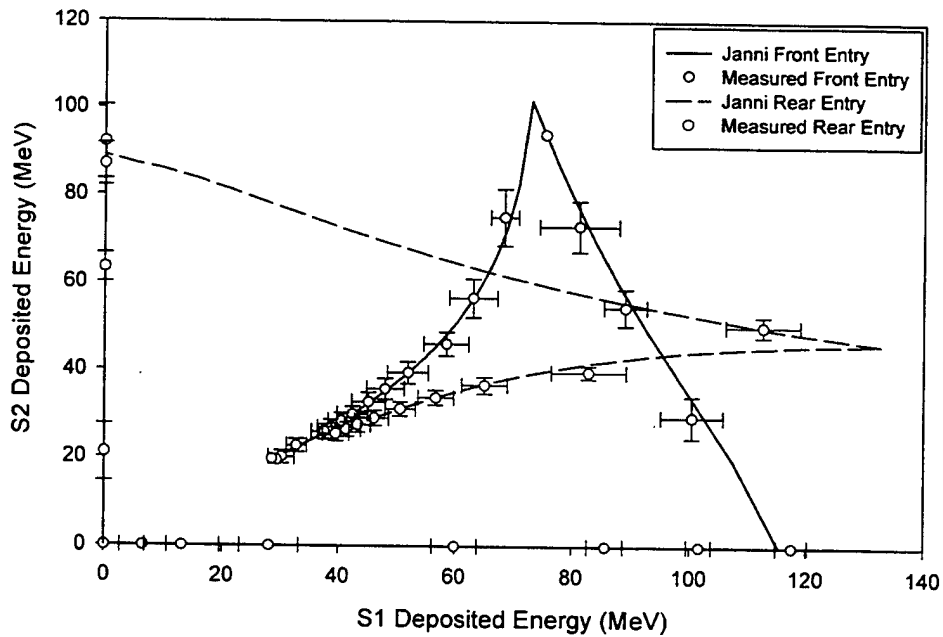
Figure 22. Plot comparing the computed and measured response in the S1S2 plane, for both front and rear entry protons.

30

PIPS Deposited Energy
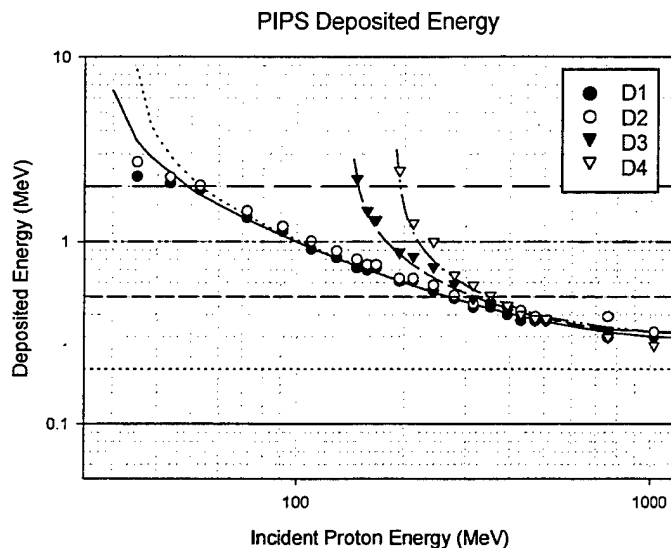
Figure 23. Plot comparing the computed response of the HEP PIPS detectors to that measured at Harvard and Brookhaven.

To obtain the energy calibration for the detectors, all of the in-aperture front entry data above 50 MeV and the rear energy data above 110 MeV were used. For each experimental run, a histogram of counts versus channel number was generated. For spectra with a symmetric peak, the centroid channel was computed, while for asymmetric peaks the peak channel was selected. This was then compared with a detailed model of the expected energy deposition in the instrument, including all of the various layers in the instrument, including the minor layers of plastic and metal contacts. This model, discussed in the previous annual report, is based upon the Janni results. The Janni model yielded deposited energy, for each case, while the experimental data yielded peak channels. A linear regression was performed between the computed depositions and the peak channels.

It was empirically determined that the best fit was obtained using a 3% correction to the Bragg-Kleeman rule used for estimating the stopping power of the GSO. As discussed above, the Bragg-Kleeman rule is only valid to about 10%, so this correction is reasonable. Data taken previously with the Engineering Model indicated a 5% correction. In addition to measuring the overall response, the properties of the scintillation detectors were measured, including the light yield, electronic noise, and total resolution. To obtain the light yield, the PIN photodiodes were exposed to gamma sources (^{137}Cs, ^{60}Co) and the photopeaks and Compton edges measured. This provided an absolute calibration of the MCA output, in electron-hole pairs per channel. The calibration of the energy response described above provided the MeV deposited per channel. From these two, the number of electron-hole pairs per MeV was deduced. To obtain the electronic noise, a test pulser was used. Table 3 is a summary of the results.

31

Table 3. Summary of scintillator calibration results

	Light Yield (elec.-hole pairs/MeV)	Electronic Noise (MeV FWHM)	Correlation Coeff.
S1	4,470	0.7	0.997
S2	4,740	0.6	0.999
S3	2,410	1.1	0.969

The energy resolution of the scintillators was measured to be approximately 3.0 MeV for S2 and 4.2 MeV for S1, at incident energies around 500 MeV. The electronic noise, 0.6 and 0.7 MeV respectively, is negligibly small since the peak broadening terms add in quadrature. As discussed above, the dominant term in scintillator resolution is the broadening due to Landau fluctuations in the energy deposition process.

Instrument Response to Nuclear Interactions

As stated previously, inelastic nuclear scattering is an inevitable and important part of proton interactions at these energies. A model of the instrument response, including nuclear scattering, was developed using the LAHET Monte Carlo simulation code. From this model, we can deduce both the fraction of incident protons that are correctly binned and also the pattern of energy deposition in the S1S2 plane. This model was used to design the instrument, to optimize shielding and detector geometry. This model will also be very important for use in analyzing flight data. Data obtained at the AGS were used to verify this model. For example, Table 4 shows measured and computed results obtained at 510 MeV. The first column shows that, for protons incident at 510 MeV, approximately 80% of those triggering D1 and D2 are correctly measured by the energy channels set using the Bethe-Bloch approximation. As shown in the second column, approximately 2% trigger the "C" logic (all four SDs) but have an energy deposition pattern not matching the Bethe-Bloch approximation. These will not be counted by the nominal channels, but will be counted by background data channels. Similarly, 6% trigger the "B" logic (D1, D2, D3, but not D4) and 5% trigger the "A" logic. In these cases, the incident protons inelastically scatter in S2 and S1, respectively, emitting either a neutron that escapes the instrument without interacting or emitting a proton along a trajectory that does not reach D4 and/or D3. Approximately 1% of the incident 510 MeV protons will be erroneously measured in "B" energy channels (135 to 180 MeV), while approximately 5% will be erroneously measured in "A" energy channels (25 to 135 MeV). Note that 5% of the protons trigger a response in S3, presumably due to the emission of low energy protons at large angles.

Figure 24 is a plot comparing the measured and computed patterns of energy depositions due to nuclear interactions on HEP at 250 MeV. These are scatter plots of the S1S2 pulse heights corresponding to false "B" logic: events triggering D1, D2, D3 but not D4, which can only occur with a nuclear interaction. An empirical broadening of 3 MeV FWHM was added to the simulation result, to account for the finite scintillator resolution.

The excellent agreement between the measured pattern and that predicted by the LAHET simulation code is clear from Figure 24 and Table 4. The measured and modeled results were compared at nine energies between 150 and 510 MeV, with similarly good agreement. This implies that the model can be used for data analysis purposes, to compute correction factors with

a high degree of confidence. As a first order correction, the number of counts measured in each channel can be scaled up by an appropriate factor corresponding to the fraction of events lost by nuclear scattering. This correction factor can be verified by measuring the count rates in the background channels. A second order correction would use the measured counts in the highest energy channels to correct the measured counts in the lower energy channels. Because the energy spectrum drops off quickly with increasing energy, this will generally be a small correction.
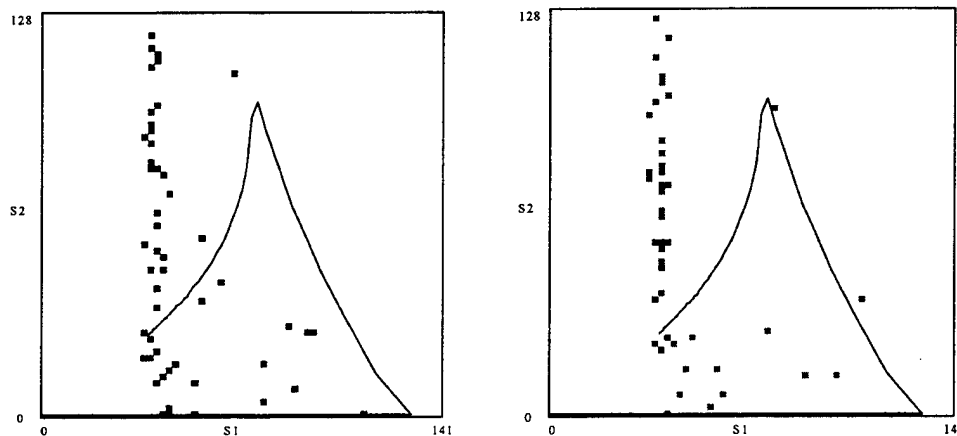
Figure 24. Measured (left) and simulated (right) S1S2 pulse height distributions for protons undergoing nuclear interactions, incident at 250 MeV. The solid line represents the deposition pattern shown in Figure 3, while the dots are a scatter plot of observed deposition values.

Table 4. Measured and computed effects of inelastic nuclear scattering at 510 MeV.

	Correct Channel	"C" Logic	"B" Logic	B Channel	"A" Logic	A Channel	S3 Veto
Measured	77.6%	81.0%	6.3%	1.0%	4.9%	4.5%	5.0%
Model	80.1%	81.6%	7.2%	1.3%	4.8%	4.0%	5.1%

Nuclear interactions in the shielding of the instrument and spacecraft will also cause some response in the instrument. During calibration at HCL, the 160 MeV proton beam was highly collimated and directed parallel to the instrument axis but offset from the aperture, along the copper collimator. No primary beam was incident through the aperture. No valid proton counts were observed, but singles counts were observed in all detectors, with a rate proportional to detector volume. This was presumably due to neutrons produced by inelastic nuclear scattering in the shielding and in the beam collimators, since neutrons can pass throughout the instrument with a small probability of interaction in each detector. Some electrons were recorded in this configuration, presumably due to neutron decays near the instrument aperture. No quantitative modeling of the consequences of inelastic nuclear scattering in the shield on the primary measurements has yet been carried out.

Off-Axis and Out of Aperture Response

The response of HEP to protons off the instrument's symmetry axis can be classified as falling into three distinct angular regimes. First, one can consider the response for angles within the nominal angular acceptance cone. At energies above 185 MeV, the response is relatively simple. For angles between 0° and 6°, protons incident anywhere over D1 will pass through all detectors and be correctly recorded. For somewhat larger angles, between 6° and 11°, an increasingly small fraction of the D1 area is projected onto the D4 active area. Thus the geometric response is essentially flat to 6° and then decreases essentially linearly to 11° off-axis. Measurements of the flux of cosmic ray muons penetrating to sea level have confirmed the computed geometric factor for the highest energy particles.

At lower energies this response is more complicated. For the highest energy type A protons, which stop near the back of S1, the acceptance cone is defined by the size of the collimator, the radius of S1, and the separation between the collimator and the rear of S1. Protons at greater angles pass through S3 and so are vetoed. Lower energy type A protons stop at a fraction of the thickness of S1. If incident at a large angle, these will still stop in S1 so will not reach S3. The separation defining the acceptance geometry is between the collimator and the stopping depth, thus the acceptance angle is larger for lower energy protons, so the geometric factor increases at lower proton energies.

Second, one can consider the response to protons which pass slightly outside of the nominal acceptance cone, with trajectories through the collimator, out to 30° off-axis. Protons below 130 MeV will be stopped by the collimator. Protons incident at slightly higher energies will lose energy in the collimator and will therefore be incident on the detector stack at a lower energy, i.e. the sensor will respond to them as lower energy protons. At most energies and angles this response is minimal, due to the S3 veto shield and the shape of the Bragg peak. However, there does exist a narrow angular range between 15° and 20° off-axis where protons can pass between D3 and S3. High energy protons incident along these trajectories will be recorded incorrectly as type A protons. This is a relatively small effect, due to the narrow angular acceptance range and the steeply falling proton energy spectrum. Moreover, the same proton population which produces these false "A" events will also produce events with energy depositions consistent with type A events, but will trigger the type B and type C logic. Because HEP measures these events in the background data channels, HEP will directly measure the particle population causing these false "A" events, permitting correction factors to be measured. Previous instruments required an unmeasurable estimate of this correction, adding significantly to measurement uncertainty.

Figure 25 shows both the computed and measured response of HEP to off-axis 330 MeV protons. The solid curve shows the computed in-aperture response, in the nominal channel, which is flat to about 6° then decreases to about 11°. The peak value, 80%, is due to nuclear scattering effects. The diamonds show measured values, in good agreement. The dashed line shows the computed response in the type A channels, showing the effects of collimator penetration, with measured values shown using circles. Importantly, the complete response vanished at 30° off axis.
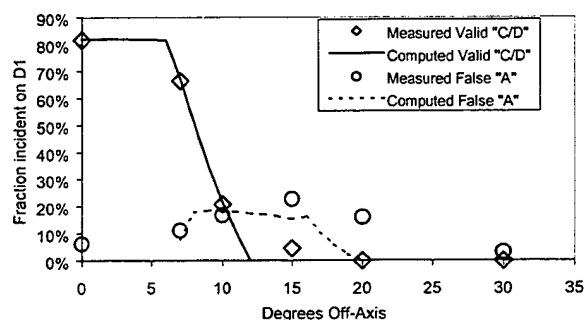
Figure 25. Comparison of the measured and computed off-axis response to 330 MeV protons.

Third, one can consider the response to angles more than 30° off axis. At these large angles, there are no trajectories that can simultaneously trigger multiple detectors and thus cause false counts. The only consequence of these protons is to produce a relatively high singles rate of non-coincidence events in each detector. Beam calibrations verified that the minimum energy required to penetrate the side, rear, and front shielding is 60, 100, and 130 MeV, respectively. It should be noted that the presence of the spacecraft will significantly affect the flux of protons incident at large angles.

2.6 FLIGHT ELECTRONICS BOX DESIGN, FABRICATION, AND CALIBRATION

Once the protoflight and flight sensors had been fabricated and calibrated, the electronics box was designed, fabricated, and calibrated. The measured performance of the sensor head drove the requirements for the electronics box. There are three major subsystems within the electronics box: analog electronics, digital signal processing electronics, and spacecraft interfacing systems. The spacecraft interface includes the CPU, a communications interface, the power supply, and the mechanical structure.

The analog electronics largely filter and amplify the analog signals from the sensor head, then digitize them for further processing. The digital signal processing electronics (DSP) determine when a valid proton event occurs and bin the event according to the preset logic masks and lookup tables. The output of the DSP is a set of histograms that represent the number of counts meeting the specified criteria during the preceding acquisition interval. The CPU periodically reads selected portions of the DSP outputs and formats the data from transmission to the ground, summing data internally and compressing it as required.

The analog circuitry used to process the detector outputs is split between the sensor head and the electronics box.. Schematics of the electronics were shown previously, in Figure 19 and Figure 20, and the design discussed there. For the PIPS detectors, the electronics box contains only the quad threshold. For the scintillators, the electronics box contains the low pass filtering and the peak hold hybrid, for S1 and S2, and the crossover timing discriminator, for S3. The most important properties of the design, such as the noise performance, were discussed previously.

A block diagram of the HEP digital electronics is shown in Figure 26. There are two major components: a digital signal processing (DSP) portion and a microprocessor portion. The inputs to the DSP are (1) four timing signals, one from each of the D1-D4 detectors; (2) three pulse height analysis (PHA) signals from each of the D1-D4 detectors; (3) a timing signal from the S3

35

scintillator; (4) the analog shaped signals from the S1 and S2 scintillators; and (5) a trigger signal from the S1 and S2 scintillators.
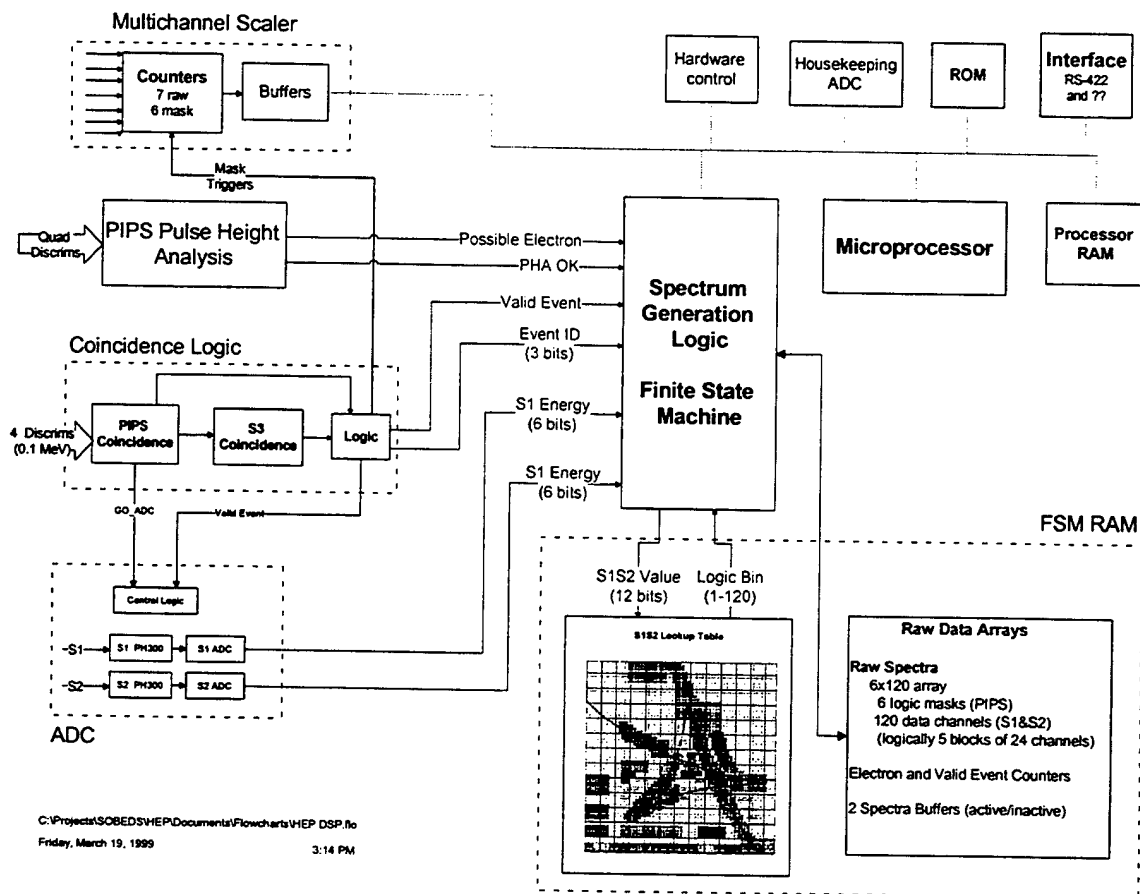
Figure 26. HEP Digital Electronics

A particular pattern in the D1-D4 and S3 detectors (termed trigger detectors) is called a **logic mask.** At any one time, six patterns can be selected, commandable from the ground. Each of the 120 **output channels** is associated with a given set of (S1,S2) values, a region in the (S1,S2) plane. The channel numbers are associated with the two-dimensional S1S2 amplitude pattern, while the logic mask is associated with the trigger detector pattern. It is the combination of the logic masks and channel number that identifies the origin of the protons.

The primary output from the DSP is a set of six 120 element histograms, each representing the number of events which (1) match one of 6 predefined patterns for the D1-D4 and S3 detectors and (2) have pulse heights in the S1 and S2 scintillators within one of 120 ranges. The secondary output from the DSP is the raw count rates in all seven detectors, of electrons, and of pattern matches. The microprocessor reads data from the 6x120 array, reads the 15 counters, sums the data for 1 second, formats the data, and telemeters it to the spacecraft. As currently configured, the processor reads the data in 24 channel blocks, reading up to 12 blocks at a time.

2.6.1 Digital Signal Processing

The Digital Signal Processing (DSP) circuitry implements six major functions. All of these DSP functions were implemented using Actel 1020A field programmable gate arrays (FPGAs). These are fast, low power, radiation hardened devices. The DSP is critical to the proper operation of HEP and its design was a major effort.

36

The first DSP function is the **coincidence logic**: the primary purpose of the coincidence logic is to determine if the D1-D4 and S3 detectors were triggered, within a 100 nsec timing window, with a pattern that matched one of the six defined logic masks. If there was such a match, then the rest of the processing proceeds. The coincidence logic also initiates the S1 and S2 ADC if a possible event occurs. Because the event processing can take considerable time, if other valid events occur while an initial event is being processed, the coincidence logic identifies and counts such matches. The outputs of the coincidence logic are (1) an *Event Trigger*, signaling that a valid event occurred, (2) an *Event ID*, a three-bit value indicating which of the six logic masks was matched, (3) a *Go ADC* signal to start the S1 and S2 ADC, (4) six *Mask Match* signals that are set if the corresponding mask is matched, and (5) a *STROBE* signal telling when the *MaskMatch* signals are valid.

The second DSP function is the **PIPS Pulse Height Analysis**: the primary purpose of the PIPS PHA is to verify that the pulse heights in the D1-D4 detectors are consistent with that expected for given proton energy ranges, determined by the logic masks. The secondary purpose is to identify when the pattern of energy deposition and D1 and D2 are consistent with the energy of an energetic electron. The outputs of the PIPS PHA are (1) a *PHA OK* signal, which indicates that energy deposition is consistent with the logic mask, and (2) an *Electron* signal, indicating that energy deposition was consistent with an electron. The PIPS PHA signal can be forced by command to be continuously OK, i.e. the PIPS PHA can be disabled.

The third DSP function is the **Analog to Digital Converter**: the purpose of the ADC is to digitize the S1 and S2 peak amplitudes when a valid event occurs. Note that we regard the ADC circuit for the S1 and S2 scintillators as part of the DSP, while the PHA analog to digital conversion for the D1-D4 detectors was discussed previously. This is because the S1 and S2 ADC includes considerable digital logic. The outputs of the ADC are two six bit values, representing energy deposited in S1 and S2, respectively. The fourth DSP function is the **S1S2 Lookup Table**. Each of the 120 output channels is associated with a given region in the (S1,S2) plane. The lookup table takes as input the 12 bit S1S2 value and produces as output a number from 0 to 119 indicating the output channel number. The output is 0 for events to be ignored.

The fifth DSP function is the **Spectrum Generation Logic**: the primary purpose of the spectrum generation logic (SGL) is to produce the six, 120 element histograms from the Event ID, which indicates in which of the six histograms a particular event belongs, and from the S1S2 Lookup channel number, which indicates in which of the 120 channels a particular event belongs. The histogram is updated only if the PIPS PHA value is valid. The secondary purpose of the SGL is to identify electrons, using the combination of the Electron signal from the PIPS PHA and the output channel number. The SGL maintains two separate 6x120 arrays, one of which is active at all times. The microprocessor commands the SGL to switch buffers, reads the data out of the inactive buffer, and clears the data in the inactive buffer before switching back. The output of the SGL is the 6x120 element array.

The sixth DSP function is the **Multichannel Scaler**: its purpose is to count fourteen types of events. It counts the raw signal rate in each of the seven detectors, the number of times each logic mask is matched, and the number of times an Event Trigger is generated. These fourteen values are read by the microprocessor and reset at microprocessor command.

Coincidence Logic

The Coincidence Logic is a critical piece of the HEP processing scheme: only if this circuitry determines a coincidence does the rest of the data processing commence. Its timing is critically important in determining the window for accepting valid events, and for determining the accidental coincidence rates, dead time, and so on. The timing constraints imposed by the detectors and analog electronics make the timing characteristics and operation non-trivial. The timing properties cannot be described using a single timing window for all classes of events. Instead, there are distinct timing windows for valid events, for rejected events, for events rejected by S3 vs. D1-D4, and so on.

The general operation of the coincidence logic is shown in Figure 27. When a signal occurs on any of the D1-D4 triggers, coincidence processing begins and a GO ADC signal is generated (not shown). If there is a valid coincidence among these four, matching any of the six commandable logic masks within 100 nsec after the first signal is received, then these values are latched and a 50 nsec delay is generated. After this delay, a 160 nsec timing window opens for S3. At the conclusion of this interval, if a proper match is found with all five trigger detectors, then the Event Trigger and Event ID are generated.
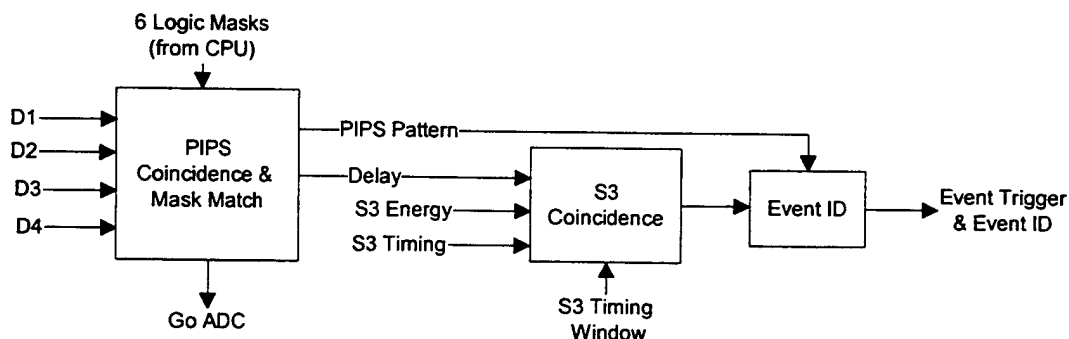
Figure 27. Block diagram of the coincidence logic

This circuitry is implemented in an Actel 1020A FPGA, which provides low power consumption and radiation hardness. This circuit is fully asynchronous, to provide the needed timing resolution. It uses pipelined logic, so that the PIPS coincidence is rapidly reset to record additional coincidences, even while subsequent event processing is in progress. The timing windows are largely determined from passive delay lines, which are very stable, radiation hard, etc.

The coincidence window length was carefully measured as 100 nsec. The maximum timing walk of the PIPS signals was measured as 50 nsec. The timing jitter has a maximum 6 nsec FWHM. Timing properties were shown to change by less than 10 nsec due to changes in temperature, supply voltage and so on. The coincidence window thus has an adequate design margin.

Figure 28 shows measured accidental coincidences and vetoes, obtained using random tail pulsers. Figure 28 (a) compares the measured and computed accidental coincidence rate obtained with two random pulsers into two PIPS detectors. The accidental rate is low at the expected count rates, a few thousand counts per sec, and matches very well with that predicted for a 100 nsec window. Since HEP measures the raw rates, the accidental rate will be known and the "background" effect can be removed during data processing. Figure 28 (b) compares the measured and computed rate of false vetoes due to signals in S3. A periodic pulser was injected

into D1, D2, and S1, and a random pulser into S3. At the maximum singles rate expected in S3, 150,000 sec-1, the false veto rate is 1.5%.

Measured Accidental Coincidences
Computation: 100 nsec PIPS window

Measured Accidental Vetoes
Computation: 90 nsec S3 Window
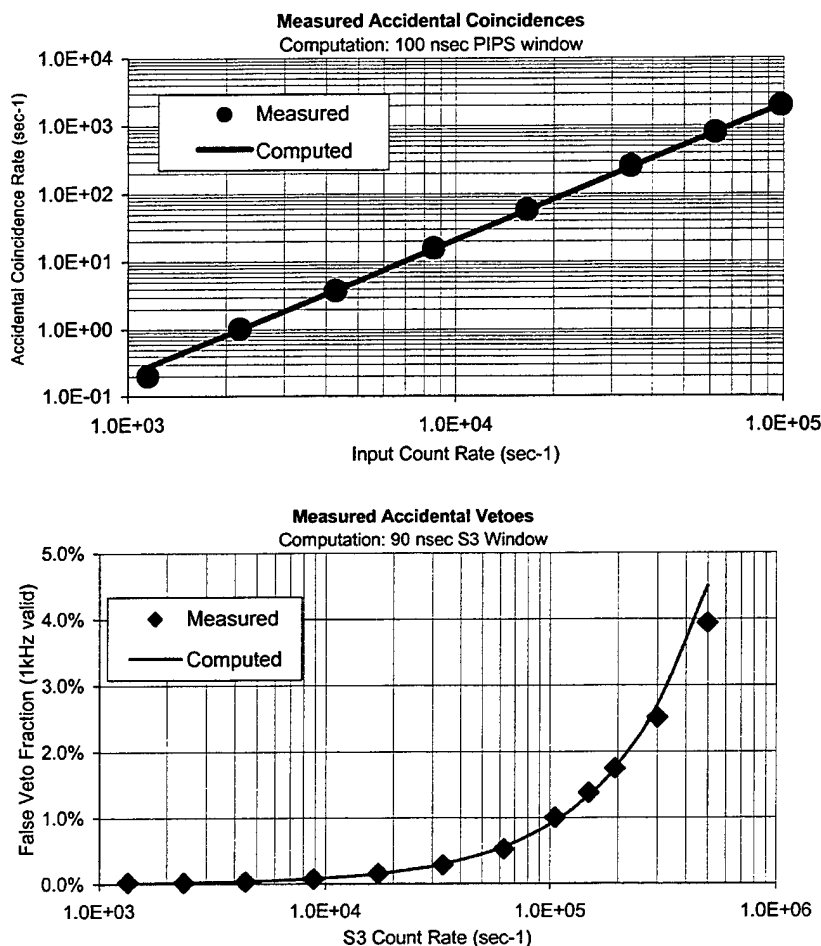
Figure 28. Plots showing the measured performance of the coincidence circuitry. The rate of accidental coincidences and vetoes is small and matches that computed from circuit design parameters.

Multichannel Scaler

The HEP hardware scalers count the number of events. There are fourteen hardware scalers. Each of the seven detectors has a scaler, which counts the number of times a low level comparator is triggered. Each of the six logic masks has an associated scaler, and the "Event Trigger" indicator from the Coincidence Logic has a scaler, although only events entering the subsequent processing chain are counted here, meaning that this scaler may show a smaller value than the sum of the logic mask scalers, even if the logic mask scalers are mutually exclusive.

The counters have variable depth, based upon the rate that is expected on orbit. For the raw rates in the detectors, the counter depth is sufficient to handle a rate at least five times that expected from the AP8 worst case model. For the logic masks, it is vastly higher than the maximum expected rate of real, in-aperture events. The maximum expected rates, number of bits, and maximum measurable rates are shown inTable 5. The CPU reads out the scalers at a 10 Hz rate.

39

Table 5. Counter depths.

	Max AP8 Rate	Bits	Max Rate in cps
D1, D2	1,975	8 + 4 = 12	40,960
D3	6.619	8 + 6 = 14	163,840
D4	22,310	8 + 8 = 16	655,360
S1, S2, S3	138,400	8 + 8 = 16	655,360
"Event Trigger"	Singles: 22.310	8 + 4 = 12	40,960
Mask Counter 1	Real: 144	8 + 8 = 16	655,360
Mask Counters 2 to 6	Real: 144	8 + 4 = 12	40,960

Figure 29 shows the performance of the multichannel scaler at high count rates. The D1, D2, D3, and D4 counter depths are based upon the maximum count rates expected in orbit, shown along the bottom axis. In each of these detectors, the observed count rate matches the input rate up to the maximum and then is flat for all higher count rates. For the scintillators, the measured count rate deviates somewhat from the input rate due to pulse pile-up. However, this deviation only occurs at count rates well above that expected on orbit (150,000 sec^{-1}) and is well matched by that computed from the known pulse widths.

HEP Prototype Scaler Random Pulser Tests
Boxes show max expected from isotropic AP8
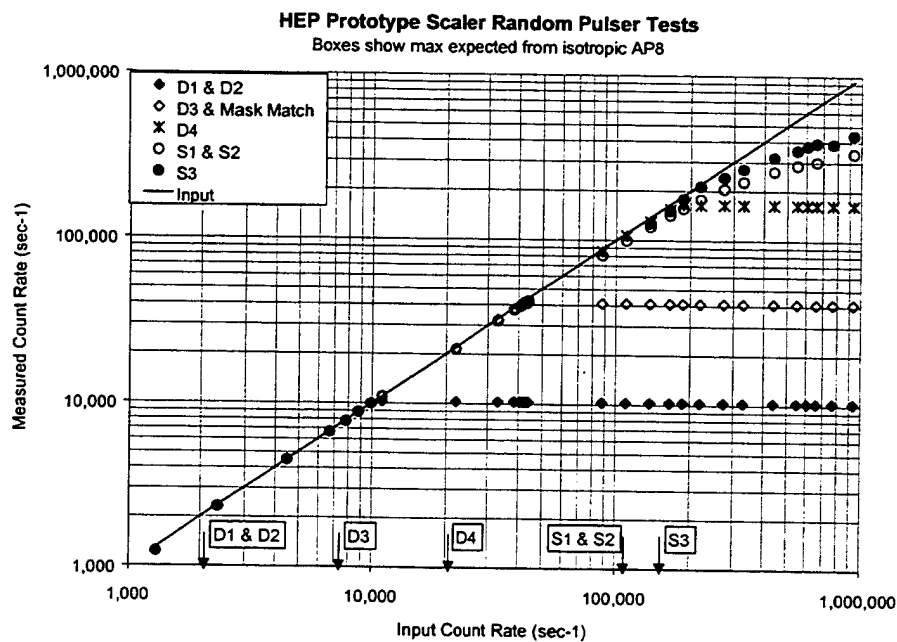
Figure 29. Measured performance of the HEP scalers at count rates up to 10^6 sec^{-1}.

Electron Counter

Although HEP is designed primarily to measure energetic protons, it can also be used to measure energetic electrons. Electrons with an energy exceeding about 1 MeV have a range sufficient to penetrate the copper degrader, D1, and D2. Electrons of 1-10 MeV are nearly minimum ionizing particles, so will generally deposit relatively small amounts of energy in D1

40

and D2, and will deposit little energy in the S1 scintillator. Because electrons scatter and emit Bremsstrahlung X-rays, the pattern of energy deposition is complicated but generally involves depositing little energy in D1, D2, and S1.

Protons that barely reach S1 will also trigger D1 and D2 but not deposit much energy in S1. However, these are protons near the end of their trajectory so they deposit large amounts of energy in D1 and D2. Protons that are energetic enough to have low energy depositions in D1 and D2, will however deposit a significant amount of energy in S1. Therefore, we can use the combination of pulse height analysis on the PIPS signals and on S1 to distinguish energetic electrons from protons.

A portion of this is implemented in the PIPS PHA circuitry. A "Possible Electron" flag is set by the PIPS PHA circuitry if the energy depositions are:

$$0.16 < D1 \ \& \ D2 < 2.1 \qquad D3 < 0.1 \qquad D4 < 0.1$$

Both electrons and some protons can meet this condition, but the protons matching this are higher energy type A protons which deposit considerable energy in S1. The Spectrum Generation Logic, described below, combines this flag with the S1S2 look-up table (LUT) to distinguish electrons and protons. Specifically, if the "Possible Electron" flag is true and the S1S2 LUT indicates channel 1 (both S1 and S2 depositions below a threshold), then the electron counter is incremented. If the S1S2 LUT indicates a channel other than 1, then the "Possible Electron" flag is ignored.

Digitizer and Lookup Table

The S1 and S2 digitizers are based on a Wilkinson ADC. The peak amplitude of the pulse is held on a capacitor, using a peak hold circuit. The ADC then injects a fixed current and measures the time required to discharge the capacitor. The discharge time is obviously proportional to the charge, i.e. the voltage. In HEP, there are two ADCs, one for S1 and one for S2. Each ADC has three major function blocks: a peak detect and hold circuit, a timing circuit, and control logic. The peak detect and hold is implemented using an Amptek PH300RH hybrid. The timing and control logic portion are implemented in an FPGA as a finite state machine.

The Look-Up Table (LUT) relates the S1 and S2 amplitudes to the channel number. The LUT is stored in SEU-tolerant RAM. The inputs are the two six-bit values S1 and S2, i.e. a 12 bit word, which represents an address in a 4k block of RAM. At each address is the channel number. Several different LUTs are supported. First and foremost is the default LUT, which is the primary look-up table for flight measurements of energetic protons. Channels 0 through 23 represent front entry protons and are assigned to RAM addresses that correspond to the most probable depositions as computed from the Janni table. Channels 24 through 47 represent background protons and are assigned to detect various classes of events. No channels above 48 are assigned a value in the default LUT. The default LUT will assign all addresses not otherwise specified as channel 47. The default LUT is stored in PROM and is read into the LUT RAM when the instrument is turned on.

HEP has the capability to upload a new LUT to RAM. HEP also includes the capability to generate computed LUTs, for calibration purposes. In the "S1 LUT", the S2 digitized value is completely ignored, and the output channel number is equal to the S1 digitized value. That is, the RAM value is "01" for every address with S1=01, S2=don't care. The "S2 LUT" is similar. Sending the command to use an S1 or S2 LUT causes the CPU to compute the proper channel numbers and to write them to the LUT RAM. With the S1 LUT, one obtains the spectrum of

energy deposited in S1, regardless of what happens in S2, for each logic mask. The final computed LUT is for on-orbit calibration. One sends a command to HEP, containing as a parameter a 12-bit value corresponding to the central point in the desired calibration region. HEP then assigns output channel numbers 48 through 119 to the 72 adjacent addresses, in an 8x9 array. Each channel corresponds to a single S1S2 address. This permits one to accurately locate the minimum ionizing point, to detect any drifts in system gain.

Spectrum Generation Logic

The primary purpose of the spectrum generation logic (SGL) is to produce the 6x120 raw data array containing the information on the input proton spectrum. The inputs are (1) the Event ID, which indicates in which of the six histograms a particular event belongs, (2) the S1S2 Lookup channel number, which indicates in which of the 120 channels a particular event belongs, and (3) the PIPS PHA indicator. When a valid event trigger occurs, and if the PIPS PHA indicator is OK, then the Event ID (1-6) and the channel number (0-119) are used to identify the appropriate cell in the 6x120 raw data array. The value in this cell is incremented. There are actually two separate 6x120 arrays, one of which is active at all times. The data are incremented in the active array. The microprocessor commands the SGL to switch buffers, reads the data out of the inactive buffer, and clears the data in the inactive buffer before switching back. The SGL also identifies electrons as discussed above. The Spectrum Generation Logic is implemented in an FPGA as a finite state machine. The block diagram for the finite state machine is shown in Figure 30.
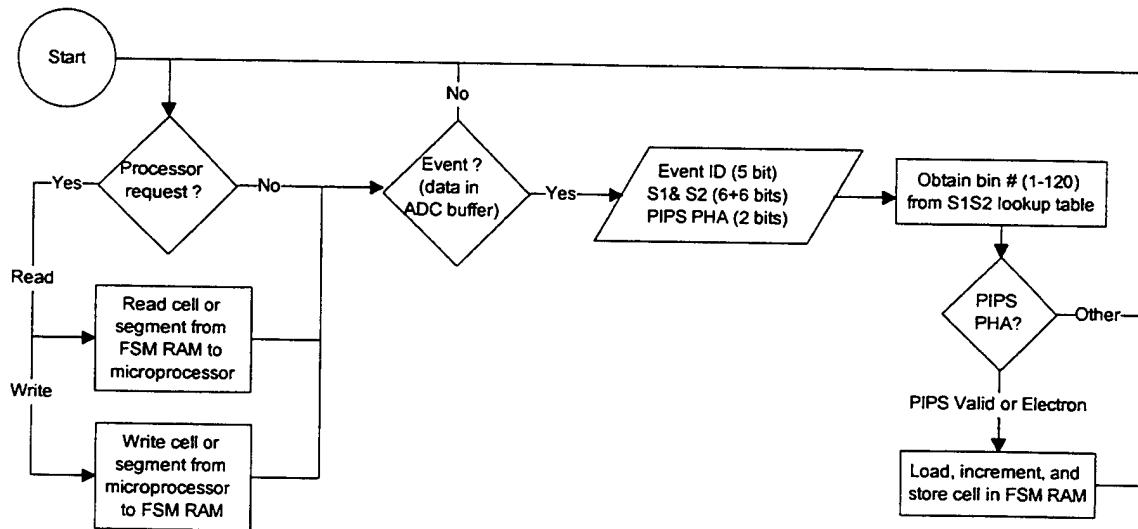
Figure 30. Block diagram of Spectrum Generation Logic finite state machine.

The finite state machine continually executes the loop shown in Figure 30. It starts by checking for a processor request to read or write to a cell in the raw data array. If there is no request, then it looks for a Valid Event Trigger. If there is a trigger, then the finite state machine reads the Event ID, channel number and PIPS PHA and increments the proper cell in the raw data array.

2.6.2   CPU and Onboard Software

The primary purpose of the HEP CPU is to read a subset of the data from the DSP (spectral array plus scalers), to sum the selected values over a readout interval, and to log compress the

summed values for telemetry. The secondary purposes of the CPU are to receive and process commands from the ground, and to handle housekeeping.

From the perspective of the CPU, certain portions of the 6x120 raw data array are designated "active". Active cells and all scalers are read out by the CPU and reset at a rate of 10 Hz, when the buffers are switched. Inactive cells are read out and reset as a background task by the CPU. Every 100 msec, the CPU must (1) command the Spectrum Generation FSM to switch buffers, (2) latch, then clear the scalers, (3) read selected cells from the FSM RAM and add these to the proper cells in the active buffer in CPU RAM, (4) read the scaler latches and add the read values to the scaler sums, and (5) zero the cells in the FSM RAM.

At present, with no flight interface specified, active cells are designed in blocks of 24 cells. That is, for each of the six logic masks, channels 0-23 form one block, channels 24-47 form a second block, and so on. There are 30 such blocks in the raw data array. The user can send a command to HEP designating any of the 30 blocks as active. At any one time, up to 12 blocks may be active. The rate at which inactive blocks are read out depends upon the time the CPU has available and so depends upon the number of active blocks. In the future, HEP will have the capability to read out individual cells and group them into a mixed block of 24 cells. The user will be able to select any cell that is part of an active block for readout into the mixed block. The active block notation describes the rate at which the CPU reads data from the DSP memory. With the current software, all active blocks are transmitted once per second, but this need not be case with the flight software. At present, the active blocks are summed in an array in CPU RAM for 1 second and then the raw values transmitted. Also transmitted are any inactive blocks that were read out, the 1-second scaler sums, and some housekeeping. The flight software will certainly differ in some details. The values will be log compressed. The readout intervals and data rates are TBD. If necessary, the CPU will do pitch angle binning but this has not yet been implemented.

The HEP CPU uses an 80C85 radiation hardened microprocessor, with an 8k-byte RAM and a custom FPGA which implements the interface with the DSP (the spectrum generation finite state machine and the scalers), the RS422 interface, and various microprocessor functions. The CPU design is a modification of that used on CEASE, with flight heritage.

2.6.3 High Count Rate Response

As noted previously, HEP will experience a high singles rate in its detectors at the peak of the radiation belts, which is where the HEP measurements are of most interest. The details of the digital design impact the instrument response at these high rates. The high singles rates will lead to three distinct effects in HEP's response: pulse-pile-up, random coincidences (which include false positives and false vetoes), and dead time losses. Pulse pile-up is only a concern in the detectors where the pulse amplitude is measured, S1 and S2. The S1 and S2 shaped pulses have an effective width of 0.5 μsec FWHM. At 100,000 sec^{-1} in each detector, approximately 80% of the counts will have no distortion in amplitude. Because much of the pile-up will involve very high energy protons passing all the way through the scintillators, along the shorter axis, there will be many low energy depositions. Moreover, HEP only has 64 channels, with several ADC channels combined into a single output data channel. Much of the pile-up will not distort the amplitude enough to change the measured energy channel. In addition, the HEP background channels will include channels dedicated to measuring pile-up events, which can only have amplitude greater than nominal. Combining this information with the measured count rates in S1 and S2 will permit very accurate pile-up corrections to be made.

43

The probability of a false random positive coincidence is extremely small because of the 100 nsec coincidence window for the SDs and the requirement for multiple coincidences. At the AP8 peak, the rate of D1 and D2 randoms will only be 0.8 sec^{-1}, with the real rate expected to be >100 sec^{-1}. If a real type B event occurs, the probability of random D4 occurring and causing an binning error is only 0.2%. Moreover, the S1S2 amplitudes will prevent such an event from being recorded as valid. In general, the probability of false positives is negligible. The most important random coincidence event is a false veto from S3, when a particle passes through S3 simultaneously with a real event. Given the 120 nsec S3 window, with timing initiated by the SDs, the false veto rate from S3 will be about 3%. Moreover, virtually all of these protons will also pass through S1 and thus lead to pulse pile-up. These random coincidence rates and window lengths were verified through the use of both random pulsers and gamma ray sources which stimulate the detectors independently. Since the raw rates in the detectors are measured, and the random coincidence rates can be directly computed from these raw rates, effects due to random coincidences can be very reliably corrected.

The electronics in HEP have dead times which lead to certain measurement effects. First, the counters measuring the raw count rates in the seven detectors have a paralyzable dead time associated with the duration of the analog signals. For the SDs, the dead time is 1.0 μsec pulse width, while for S1 and S2 it is 0.5 μsec and for S3 it is 0.25 μsec. Second, the counters measuring the coincidence logic matches have a nonparalyzable 0.24 μsec dead time associated with operation of the coincidence logic. Third, the spectrum generation logic has a dead time that is associated with the ADC operation. This dead time is variable, since the digitization time for each event depends upon the pulse amplitude. When any of the SDs is triggered, the ADC begins an acquisition cycle with a minimum duration of 1 μsec, for events rejected by the coincidence logic, and with a maximum duration of 10 μsec, for the largest digitized amplitudes. These losses are estimated to be <5% total. The rate of coincidence logic matches can be used to correct the output spectra for ADC dead time losses.

2.6.4 Spacecraft Interface

No spaceflight has been assigned to HEP, so a flexible, "generic" interface has been implemented. The serial command/telemetry interface now used is an asynchronous serial interface using RS422 hardware. The power supply uses a 28V nominal input. It is a quasiresonant, transformer coupled supply operating at a nominal 100 kHz, producing both the low voltages required for analog and digital circuitry and also the high voltages (250V) required for biasing the detectors. The I/O and power supply designs are modifications of those use on CEASE, so have flight heritage.

3 LEPDOS DESIGN AND FABRICATION

As part of the SOBEDS contract, Amptek has designed and fabricated three flight LEPDOS instruments. The purpose of the LEPDOS instrument is to measure: 1) the lower energy protons and electrons which may cause spacecraft anomalies, specifically protons from 0.7 to 80 MeV and electrons from 5 to >250 keV, 2) the dose and dose rate experienced by spacecraft electronics, 3) particles causing single event effects, and 4) to provide real-time warnings to spacecraft and operators of environmental conditions likely to cause anomalies, such as surface charging and deep dielectric charging. The overall design of the LEPDOS instrument is based on previous flight instruments and has been published previously[2].

Two major efforts were carried out on the LEPDOS instruments as part of the SOBEDS contract. First, two standard LEPDOS units where designed and fabricated. Previous designs were modified, based on lessons learned, then the flight instruments were manufactured and tested. Second, a third LEPDOS instrument was tailored for use in geosynchronous orbit (GEO) on a Defense Support Program (DSP) spacecraft. In order to measure the relevant particles (ions/electrons) particular to this orbit, an additional sensor was implemented on this LEPDOS instrument, an electrostatic analyzer to measure electrons. On-board data processing software was additionally required, with sensor calibrations.

3.1 DESIGN, FABRICATION, AND CALIBRATION OF STANDARD LEPDOS UNITS

3.1.1 LEPDOS Common Design and Fabrication

A portion of the LEPDOS design effort was shared by all of the LEPDOS units, focused on improving previous designs, based on lessons learned. First, a particle telescope is at the core of the LEPDOS instrument. Significant changes were made to the telescope to enhance manufacturability and reliability. First, the thickness of the back telescope detector was reduced from 700 μm to 500 μm in the LEPDOS instruments. The thicker material is not always available from the manufacturer and is somewhat difficult to produce, so using a thinner detector enhances manufacturability. Second, the mechanical apparatus used to hold the Si sensors inside the telescope housing was completely redesigned, to the same dimensional specifications. The new telescope design underwent random vibration testing, at levels exceeding that expected for the space instruments, and also underwent calibration at Goddard Space Flight Center to compare its response with that of the previous telescope. The response of the telescope to electrons ranging from 175 to 1,600 keV was measured. Very good agreement with model predictions was observed. The geometric response was found to be the same, as expected. The spectral response was different, as expected from the thinner back detector: particles punch through the back detector at a lower incident energy. Figure 31 shows the computed response for the LEPDOS telescopes.

---

[2] B.K. Dichter, J. O. McGarity, M. R. Oberhardt, V. T. Jordanov, D. J. Sperry, A. C. Huber, J. A. Pantazis, E. G. Mullen, G. Ginet and M. S. Gussenhoven, "Compact Environmental Anomlay Sensor (CEASE): A Novel Spacecraft Instrument for In Situ Measurements of Environmental Conditions" *IEEE Trans. Nucl. Sci.*, Vol 45, No. 6, p. 2758, December 1998
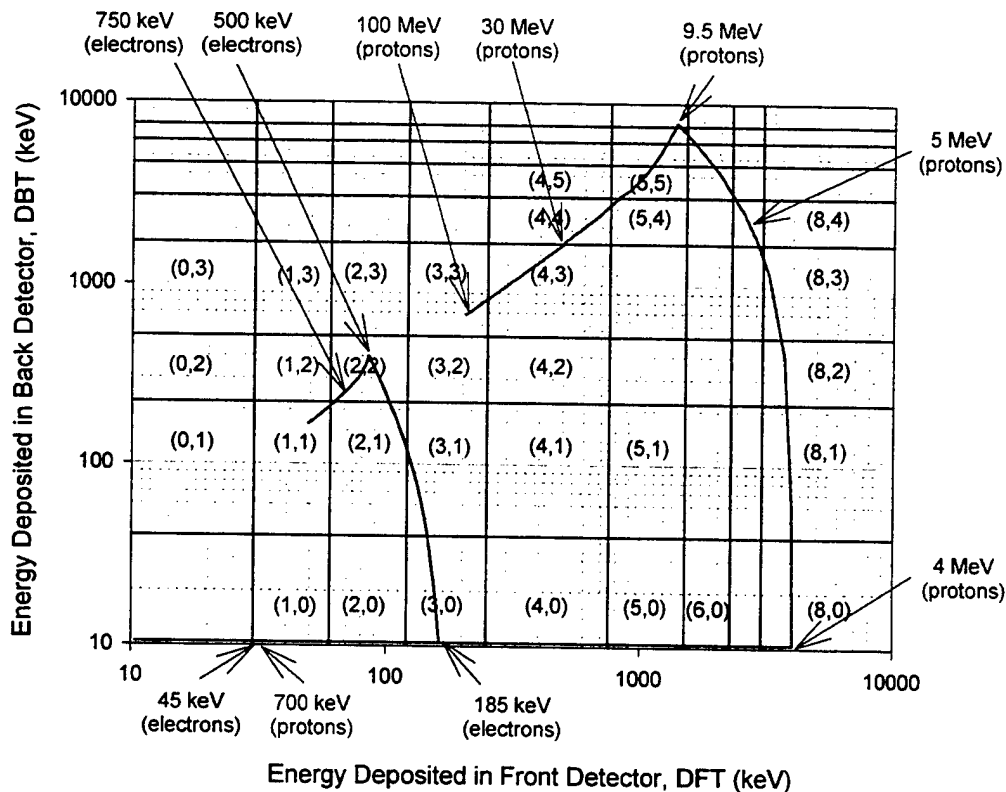
Figure 31. Plot showing the computed pattern of energy deposition in the LEPDOS particle telescope. The thresholds and the nomenclature for the Logic Boxes (LBs) are also shown.

The electronic circuitry was largely unchanged from that of the as-built CEASE units, but all of the printed circuit boards received new layouts. The final testing of the as-built CEASE units had led to various circuit modifications, which needed to be implemented in new circuit boards.

Two standard LEPDOS instruments and the tailored LEPDOS were fabricated from the new designs. The standard units are designated S/N 004 and 005 and are identical except for spacecraft specific interfaces. The LEPDOS with ESA is discussed in more detail in Section 3.2. Except for the ESA, the CPU board, and the interface, everything in this instrument (designated S/N 007) is in common with S/N 004 and 005.

3.1.2 LEPDOS Spacecraft Specific Design

As with all flight instruments, spacecraft specific design was required. One flight instrument, S/N 004, was designated by the contract monitor for flight on the SBIRS LADS spacecraft. Meeting the SBIRS LADS schedule required extremely ambitious design and fabrication efforts. The interface hardware and software were customized for this spacecraft, the instrument was manufactured, functional tests were completed, calibration was carried out, and spacecraft specific environmental tests were carried out. Shortly before this instrument was delivered, the SBIRS LADS spacecraft mission was cancelled. This instrument is now in storage at Amptek. It is anticipated that a new spacecraft specific design effort will be required when a new ride is found for S/N 004. No ride has been assigned for S/N 005, so no spacecraft specific work has been carried out. The instrument has gone through bench testing with a standard RS422 interface.

46

The S/N 007 instrument was designated to fly on the USAF Defense Support Program (DSP) Flight 21 spacecraft. This is a very mature, operational spacecraft, one in a long line of DSP spacecraft. The DSP spacecraft has a unique interface, which required significant spacecraft specific design. First, the command and telemetry interface is a custom serial interface, not built to any standard, so custom I/O hardware and software had to be designed, implemented, and tested. Moreover, there exists no standard GSE, so custom GSE hardware and software had to be designed and implemented in order to test the new instrument.

Further, the power supply on the DSP spacecraft required a custom "Power Relay Box" had to be designed, developed and manufactured to interface LEPDOS with DSP. This is a separate, spaceflight qualified piece of electronic hardware. The environmental test requirements of the DSP spacecraft exceed those of other spacecraft with which we have common experience, so a significant spacecraft specific effort was required for this unit. The complete flight instrument S/N 007 has been fabricated, calibrated, tested, delivered, is now integrated on the spacecraft, and is currently scheduled for launch in the second quarter of 2001.

3.2 DESIGN, FABRICATION, AND CALIBRATION OF LEPDOS WITH ESA

A second major technical effort on was the design and fabrication of a LEPDOS instrument customized for flight in geostationary orbit. SCATHA data indicated that spacecraft surface charging in geostationary orbit is due primarily to electrons with energies of 20 to 50 keV, with some charging due to lower energy electrons. The standard LEPDOS instruments do not directly measure the particle flux below 50 keV, but extrapolate from higher energies. The modified LEPDOS instrument includes an electrostatic analyzer (ESA) to measure directly the lower energy electron population, with energy below the threshold of the standard LEPDOS sensors.

As part of this effort, a prototype ESA was designed, built, calibrated, and the data analyzed. Based on these data, the flight ESA was designed, build, and calibrated. The rest of the LEPDOS instrument was also built. Several boards were unchanged, but a completely new CPU board was required to process data from the ESA, along with new onboard data processing algorithms.
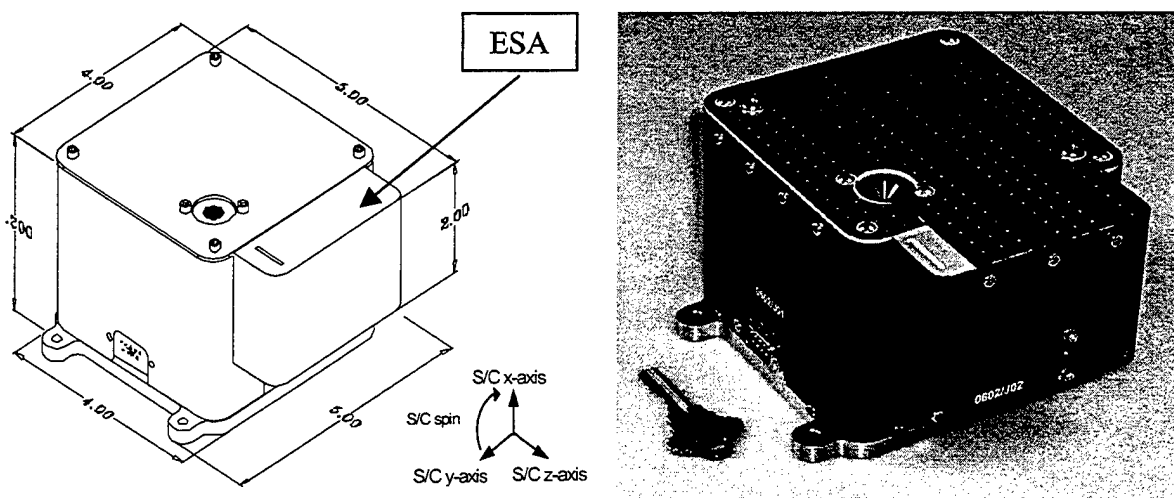

Figure 32. Drawing and photograph of LEPDOS S/N 007, which includes an ESA.

47

3.2.1 ESA Design

A drawing and photograph of LEPDOS with an ESA are shown in Figure 32. The ESA measures electrons with energies between 5 keV and 50 keV. It has an integrated angular response, relying on the isotropy of the electron population at geostationary altitudes for accurate measurements. The spectral data from the ESA are used by the LEPDOS processing algorithm to set the Surface Charging Hazard Register and associated Warning Flag. A select set of spectral data will be available in the Science Telemetry Packet and in a History Data Channel. The ESA is a modular design, which simply attaches to the side of the existing LEPDOS instrument. Few changes are required to LEPDOS: adding a connector and some counters and control logic. All of the necessary electronics, including the HV supply, are contained within the ESA on the side. This greatly simplifies the manufacturing of both standard and enhanced instruments.

Based on considerable design analysis, the basic ESA design is that of a cylindrical 125° ESA with a channel multiplier (CEM) for the sensor. This design was selected because it has significant flight experience, is straightforward to fabricate, and the performance is quite suitable for the anticipated environment. It can support a pass band from 500 eV to 50 keV, although for this particular mission the low energy cut-off was set to 5 keV.

The electronics in the ESA module include an amplifier with comparator, a customized A111F hybrid from Amptek. The ESA module also includes the HV power supply required to bias the ESA deflection plates and the CEM. A single-ended HV supply is used to simplify the design. The ESA sweeps once per second, with an exponential decay from 50 keV to 5 keV. The counts from the ESA are acquired in 25 msec bins over this energy range. The energy range is binned in 39 log-spaced steps, with the 40th bin corresponding to High Voltage Flyback. To process the data from the ESA, a counter in the CPU field programmable gate array (FPGA) accumulates the counts, which are summed for the five 1-second ESA sweeps in each SDI. The summed counts for each of the 40 bins (flyback included) are then log compressed and placed in the ESA telemetry packet. The performance of the design in the anticipated geostationary orbit was modeled to verify that the worst case environment will not swamp the electronics and the minimum environment will be accurately measured.

3.2.2 ESA Calibration

Both prototype and flight ESAs underwent extensive tests and calibrations in the MUMBO electron beam system at AFRL/VSBS. These tests validated the design, in particular the geometric factor, energy resolution, and UV rejection. Geometric calculations carried out prior to the tests predicted an energy-dependent geometric factor of 2.9×10^{-3} cm^2-ster-eV at 1 keV. The experimentally measured value was 3.1×10^{-3} cm^2-ster-eV, in excellent agreement. The measured focused and unfocussed angular responses were 2° and 8° FWHM, again in good agreement with the results of the calculations. The measured geometric factors and energy bin boundaries are shown in Table 6.

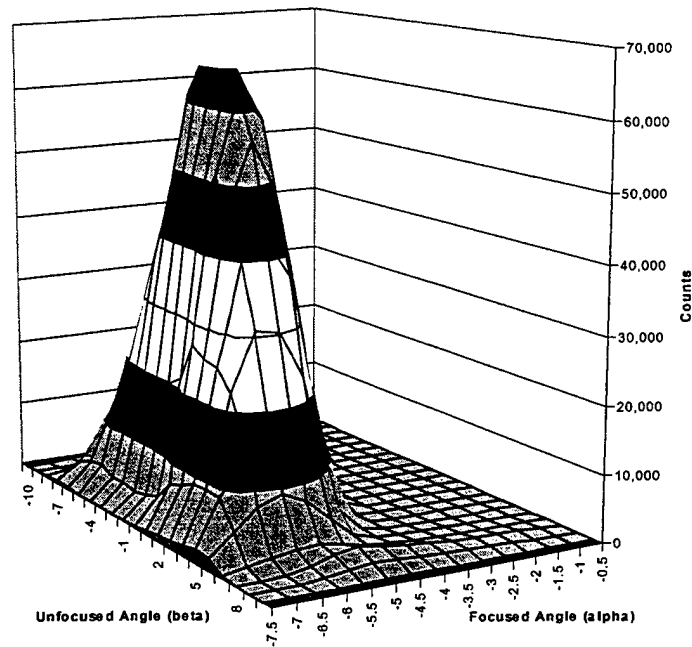Figure 33. Plot showing the measured angular response of the ESA. The angular resolution is 2° FWHM in the focused direction and 8° in the unfocused direction.
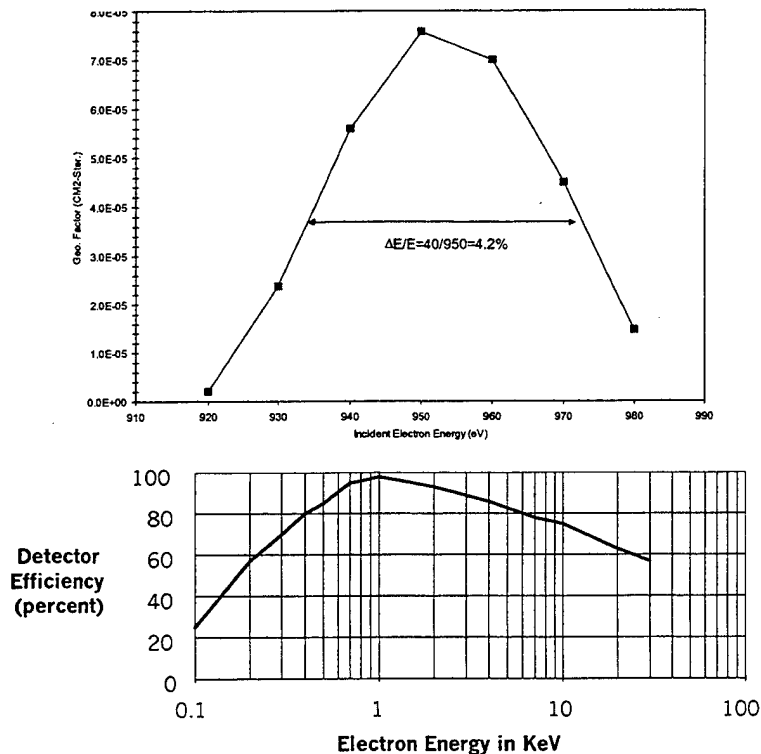

Figure 34. Top: Plot showing the measured energy passband at 1 keV. The energy resolution is 4.2% FWHM, and the geometric factor is 3.1×10^{-3} cm^2-ster-eV. Bottom: Plot showing the measured efficiency of the CEM as a function of incident energy.

49

Table 6. Measured energy bins boundaries and geometric factors for the LEPDOS ESA.

ESA Bin	GFs (cm^2-sec-sr-eV)	Center Energy (eV)	Bin Boundaries (eV) Upper	Bin Boundaries (eV) Lower	ESA Bin	GFs (cm^2-sec-sr-eV)	Center Energy (eV)	Bin Boundaries (eV) Upper	Bin Boundaries (eV) Lower
0	1.02E-01	49,271	50,749	47,793	20	8.31E-02	14,550	14,987	14,114
1	1.12E-01	46,351	47,741	44,960	21	8.05E-02	13,675	14,085	13,265
2	1.13E-01	43,604	44,912	42,296	22	7.79E-02	12,875	13,261	12,489
3	1.13E-01	41,020	42,250	39,789	23	7.54E-02	12,125	12,489	11,761
4	1.13E-01	38,588	39,746	37,431	24	7.30E-02	11,425	11,768	11,082
5	1.13E-01	36,301	37,390	35,212	25	7.06E-02	10,775	11,098	10,452
6	1.12E-01	34,150	35,175	33,126	26	6.84E-02	10,145	10,449	9,841
7	1.11E-01	32,100	33,063	31,137	27	6.60E-02	9,550	9,837	9,264
8	1.10E-01	30,200	31,106	29,294	28	6.37E-02	9,000	9,270	8,730
9	1.08E-01	28,400	29,252	27,548	29	6.15E-02	8,480	8,734	8,226
10	1.06E-01	26,700	27,501	25,899	30	5.93E-02	7,985	8,225	7,745
11	1.04E-01	25,125	25,879	24,371	31	5.72E-02	7,520	7,746	7,294
12	1.02E-01	23,625	24,334	22,916	32	5.51E-02	7,075	7,287	6,863
13	9.99E-02	22,250	22,918	21,583	33	5.30E-02	6,660	6,860	6,460
14	9.77E-02	20,950	21,579	20,322	34	5.09E-02	6,275	6,463	6,087
15	9.54E-02	19,700	20,291	19,109	35	4.90E-02	5,915	6,092	5,738
16	9.29E-02	18,510	19,065	17,955	36	4.72E-02	5,575	5,742	5,408
17	9.03E-02	17,435	17,958	16,912	37	4.45E-02	5,255	5,413	5,097
18	8.79E-02	16,450	16,944	15,957	38	4.19E-02	4,955	5,104	4,806
19	8.56E-02	15,475	15,939	15,011	39	Flyback			

3.2.3 Data Processing Hardware and Software

This customized LEPDOS unit uses the ESA data in place of telescope data to assess the surface charging hazard. The data processing hardware and software were modified to use the ESA data. The data are binned into 40 bins, summed for 5 seconds. The onboard data processing software places these values directly into the ESA Science Data packet, and also sums them to generate the Surface Dielectric Charging Status Register and Warning Flag.

For the Science Data packet, the data are log compressed (6-bit mantissa, 2 bit exponent) into one byte. The compression scheme has been chosen to accommodate expected flux levels, using SCATHA worst case instantaneous count rates and accumulating over 5 seconds in a given energy interval. To reconstruct the Counts/Bin summed over the SDI for one of the 40 intervals from the telemetry, use the following equation:

$$\text{Counts/Bin Summed over SDI} = ((M + 64.5) * 2^{E}) - 64$$

where M is the mantissa and E is the exponent.

The measured count rate, for some actual incident directional differential number flux J(E), in units of electrons/cm²-sec-ster-eV, is given by:

$$CR_{meas}(E) = J_{actual}(E) * GF * \delta E(E) * \varepsilon(E) \qquad \left(\frac{elec}{sec}\right) = \left(\frac{elec}{cm^2 - sec - ster - ev}\right)(cm^2 ster)(eV)(unitless)$$

where GF is the energy independent geometric factor, δE is the energy resolution of the ESA, and $\varepsilon(E)$ is the efficiency. We can combine these three terms into the energy dependent geometric factor, $GF(E) = GF*\delta E*\varepsilon(E)$ in units of cm²-ster-eV. This expression can obviously be inverted to obtain the directional differential number flux,

$$J_{meas}(E) = CR_{meas}(E) / GF(E)$$

The incident directional number flux over an energy range equals:

$$J_{int} = \int_{E_{min}}^{E_{max}} J(E)dE = \sum_{i_{min}}^{i_{max}} J_{meas}(E_i)\Delta E_i = \sum_{i_{min}}^{i_{max}} \frac{CR_i}{GF(E_i)}\Delta E_i$$

where the *Incident Flux* J is in units of *electrons/cm²-sec-sr*, *CR* is in *counts/sec*, *E* in *eV*, and GF in *cm²-sec-sr-eV*. and where *i* corresponds to sweep energy step, $n \geq 0$, $E_n \equiv E_{min}$, $E_0 = 50$ keV, and *GF* are the energy dependent weight factors. Note that the sum is taken over the energy sweep with bin widths of ΔE.

Parameter E_{min} is the selected minimum electron energy that contributes to spacecraft charging. The default for CEASE II will be $E_{min} = E_{26} = 10$ keV. Additional E_{min} choices available through ground commanding will be: 5, 20 and 30 keV. The weighting factors GF account for: 1) sensor detection efficiency, 2) energy channel width, and 3) sensor geometry. These factors have been determined from the ESA calibration discussed previously.

Surface dielectric charging (SDC) is the charging of externally located spacecraft dielectric surfaces by low energy electrons. By definition, the electrons responsible for SDC have very short ranges in typical spacecraft materials. Therefore, the incident flux of interest is ½ of the omni-directional flux since the spacecraft body, or other instruments, will shield the "back" side of the surface. The Effective Surface Charging Flux (F_{SDC}) in an EMI, in units of *electrons/cm²-sec*, is then:

$$F_{SDC} = 2\pi \int_{E_{min}}^{E_{max}} J(E)dE = \frac{2\pi}{\Delta T}\left\{\sum_{i_{min}}^{i_{max}} \frac{CTS_i}{GF * \delta E(E_i) * \varepsilon(E_i)}\Delta E_i\right\} = \left(\frac{2\pi}{\Delta T}\right)\left\{\sum_{i_{min}}^{i_{max}} \frac{\left[\sum_{j=1}^{60} RAW\_CTS_{ij}\right]}{GF * \delta E(E_i) * \varepsilon(E_i)}\Delta E_i\right\}$$

where ΔT is the total time that each bin is measured in an EMI, $\Delta T = 0.025$ sec * 60 sweeps = 1.5 sec. Above a threshold, B_7, for F_{SDC}, charging can be designated a hazard. The Surface Charging Hazard Register (HR_7) is a measure of the hazardous flux of low energy electrons. To compute HR_7, we define an array G_i for each B_7, and compute:

$$G_i = \left(\frac{2\pi}{\Delta T}\right)\left(\frac{\Delta E_i}{GF * \delta E(E_i) * \varepsilon(E_i)}\right)\left(\frac{1}{B_7}\right) = \left(\frac{2\pi}{\Delta T}\right)\left(\frac{\Delta E_i}{GF(E_i)}\right)\left(\frac{1}{B_7}\right),$$

$$\frac{F_{SDC}}{B_7} = \sum_{i_{min}}^{i_{max}}\left[G_i\left(\sum_{j=1}^{60} RAW\_CTS_{ij}\right)\right]$$

Threshold values for HR_7 are 0-15. HR_7 is computed as follows:

$$HR_7 = 3 * \log_{10}(F_{SDC}/B_7)$$

When the calculated HR_7 exceeds its threshold value for 3 consecutive EMI, the Warning Flag is set. The default HR_7 threshold value is 15.

4 SUMMARY AND CONCLUSIONS

The SOBEDS effort thus far has led to the delivery of four flight instruments, shown in Figure 35. The High Energy Proton telescope is a unique instrument, with an unmatched capability to measure the most penetrating protons in the Earth's radiation belts. The LEPDOS with ESA is also a unique instrument, packing a very wide variety of space environment sensors into a package several times smaller, lighter, and lower power than anything flown to date.

The second portion of the contract will cover the remaining spacecraft specific engineering, spacecraft integration, and initial flight support efforts for all four instruments. Amptek looks forward to completing this effort.
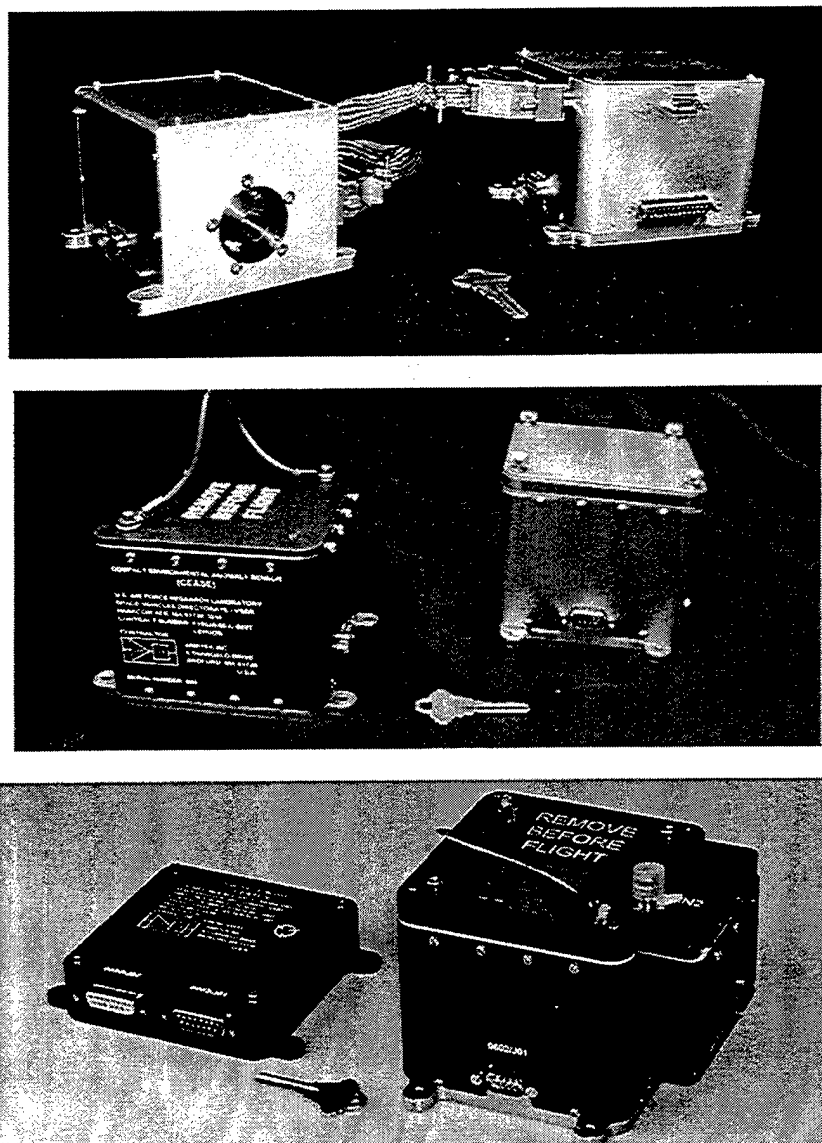

Figure 35. Photographs of spaceflight hardware developed, manufactured, and delivered under this contract. Top: HEP Sensor Head and Electronics Box. Middle: Standard LEPDOS units, S/N 004 and 005. Bottom: LEPDOS 007, with ESA, along with Relay Box.